

# Tectonics

## RESEARCH ARTICLE

10.1029/2018TC005358

### Key Points:

- Monazite ages of circa 300 Ma record peak conditions of 650 °C and 11 kbar achieved during prograde metamorphism and progressive deformation
- Late Paleozoic crustal thickening of Gondwanide basement coeval with forearc metamorphism resulted from a transpressional advancing orogen
- Low-grade metamorphism and transtension is recorded at circa 170 Ma, whereas hydrothermal activity at circa 100–80 Ma during the onset of Andean transpression is also documented

### Supporting Information:

- Supporting Information S1
- Table S1
- Table S2

### Correspondence to:

S. Oriolo,  
seba.oriolo@gmail.com;  
soriolo@gl.fcen.uba.ar

### Citation:

Oriolo, S., Schulz, B., González, P. D., Bechis, F., Olaizola, E., Krause, J., et al. (2019). The Late Paleozoic tectonometamorphic evolution of Patagonia revisited: Insights from the pressure-temperature-deformation-time (P-T-D-t) path of the Gondwanide basement of the North Patagonian Cordillera (Argentina). *Tectonics*, 38, 2378–2400. <https://doi.org/10.1029/2018TC005358>

Received 8 OCT 2018

Accepted 14 JUN 2019

Accepted article online 26 JUN 2019

Published online 16 JUL 2019

©2019. American Geophysical Union.  
All Rights Reserved.

## The Late Paleozoic Tectonometamorphic Evolution of Patagonia Revisited: Insights From the Pressure-Temperature-Deformation-Time (P-T-D-t) Path of the Gondwanide Basement of the North Patagonian Cordillera (Argentina)

Sebastián Oriolo<sup>1</sup> , Bernhard Schulz<sup>2</sup>, Pablo D. González<sup>3</sup>, Florencia Bechis<sup>4</sup>, Ezequiel Olaizola<sup>4</sup>, Joachim Krause<sup>5</sup>, Emiliano M. Renda<sup>1</sup>, and Haroldo Vizán<sup>1</sup>

<sup>1</sup>CONICET-Universidad de Buenos Aires. Instituto de Geociencias Básicas, Aplicadas y Ambientales de Buenos Aires (IGEBA), Intendente Güiraldes 2160, C1428EHA, Buenos Aires, Argentina, <sup>2</sup>Institute of Mineralogy, Division of Economic Geology and Petrology, TU Bergakademie Freiberg, Freiberg, Germany, <sup>3</sup>Instituto de Investigación en Paleobiología y Geología (UNRN-CONICET), General Roca, Argentina, <sup>4</sup>Instituto de Investigaciones en Diversidad Cultural y Procesos de Cambio, CONICET-Universidad Nacional de Río Negro, San Carlos de Bariloche, Argentina, <sup>5</sup>Helmholtz-Zentrum Dresden-Rossendorf, Helmholtz Institut Freiberg für Ressourcentechnologie, Freiberg, Germany

**Abstract** Combined field structural analysis with in situ electron probe microanalysis Th-U-Pb monazite dating, petrologic, and microstructural data provides a reconstruction of the pressure-temperature-deformation-time (P-T-D-t) path of the Gondwanide basement of the North Patagonian Cordillera. For samples from the Challhuaco hill, the timing of development of the metamorphic S<sub>2</sub> foliation and associated L<sub>2</sub> lineation and tight to isoclinal F<sub>2</sub> folds is constrained by monazite ages of 299 ± 8 and 302 ± 16 Ma during peak metamorphic conditions of ~ 650 °C and 11 kbar, achieved during prograde metamorphism and progressive deformation. Metamorphism and deformation of metamorphic complexes of the North Patagonian Andes seem to record Late Paleozoic crustal thickening and are coeval with metamorphism of accretionary complexes exposed further west in Chile, suggesting a coupled Late Devonian-Carboniferous evolution. Instead of the result of continental collision, the Gondwanide orogeny might thus be essentially linked to transpression due to advancing subduction along the proto-Pacific margin of Gondwana. On the other hand, second generation of monazite ages of 171 ± 9 and 170 ± 7 Ma constrains the timing of low-grade metamorphism related to kink band and F<sub>3</sub> open fold development during Jurassic transtension and emplacement of granitoids. Finally, a Cretaceous overprint, likely resulting from hydrothermal processes, is recorded by monazite ages of 110 ± 10 and 80 ± 20 Ma, which might be coeval with deformation along low-grade shear zones during the onset of Andean transpression.

### 1. Introduction

The Late Paleozoic Gondwanide orogen was early recognized in central Argentina by Keidel (1938 and references therein), allowing to establish one of the pioneer geologic correlations across the Atlantic Ocean. However, the tectonic significance of this key orogenic event is still under debate and has been alternatively attributed to collisional or accretional tectonics (e.g., Gregori et al., 2008, 2016; Heredia et al., 2017, 2018; Hervé et al., 2016; Pankhurst et al., 2006; Prezzi et al., 2018; Ramos, 2008; Varela et al., 2015; Vizán et al., 2015, 2017; von Gosen, 2003). These proposals have in turn led to contrasting hypotheses about the origin of the North Patagonian massif, for which an allochthonous, autochthonous, or para-autochthonous origin has been inferred (Castillo et al., 2017; Dalla Salda et al., 1992; González et al., 2011, 2012, 2018; Gregori et al., 2008; Heredia et al., 2018; Pankhurst et al., 2006, 2014; Ramos, 1984, 2008; Ramos & Naipauer, 2014; Rapalini et al., 2010, 2013).

In the particular case of northwestern Patagonia (Argentina), most contributions focused on the Late Paleozoic magmatism (Castillo et al., 2017; Cerredo & López de Luchi, 1998; Pankhurst et al., 2006; Urraza et al., 2011; Varela et al., 2005, 2015), whereas constraints on the timing and characteristics of contemporaneous deformation and metamorphism are scarce (Figure 1; Giacosa et al., 2004; von Gosen & Loske, 2004; García-Sanseguno et al., 2009; von Gosen, 2009; Martínez et al., 2012; Urraza et al., 2015).

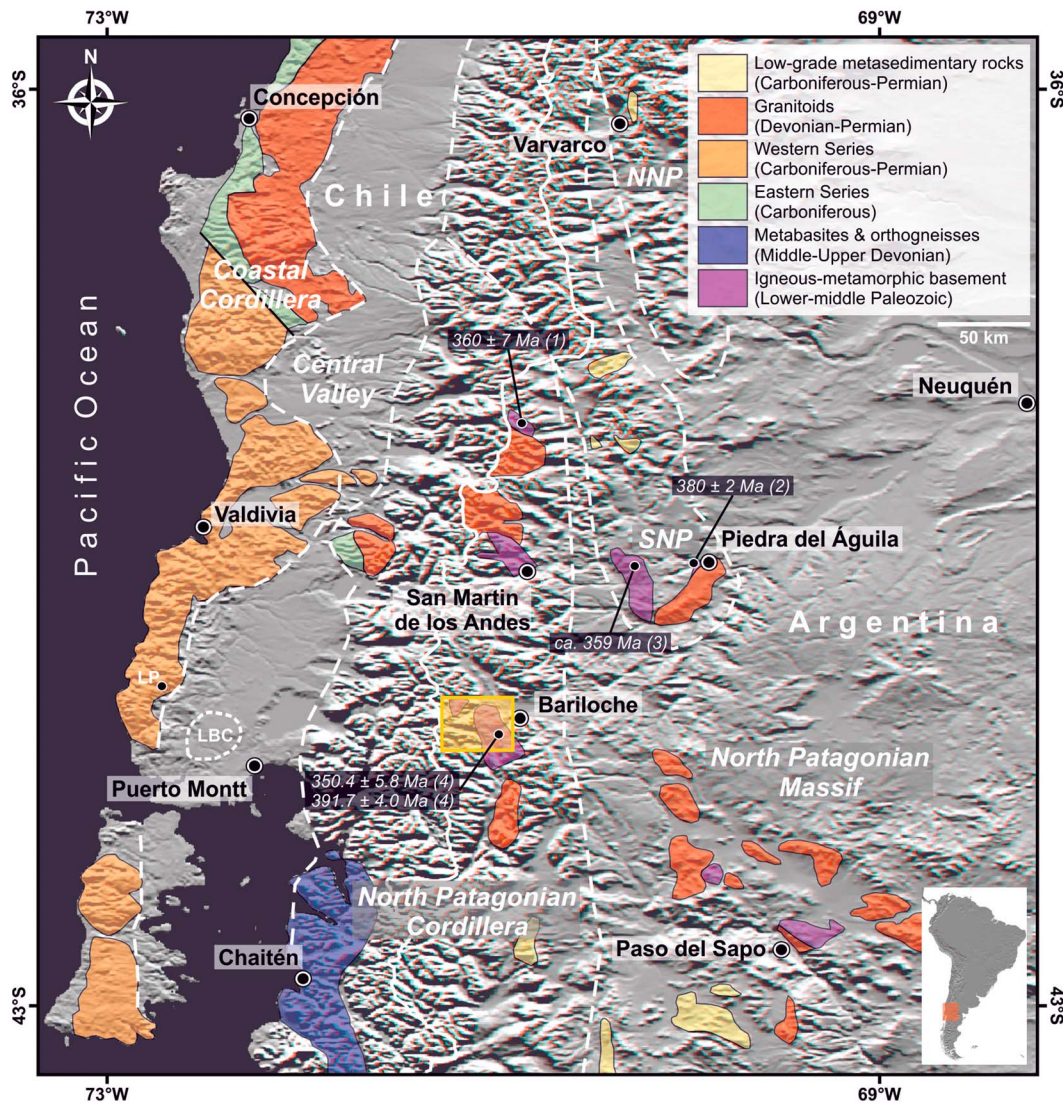


**Figure 1.** Sketch map showing main exposures of Paleozoic basement rocks in northwestern Patagonia (modified after Cingolani et al., 2011; Hervé et al., 2013; Serra-Varela et al., 2018). Inset shows area of the map in South America, whereas the yellow rectangle indicates location of the map of Figure 2. Main morphostructural units are indicated with dotted white lines (modified after Bechis, Cristallini, et al., 2014; Bechis, Encinas, et al., 2014; Ramos et al., 2011): Coastal Cordillera, Central Valley, North Patagonian Cordillera, North Patagonian Massif, Southern Neuquén Precordillera (SNP), and Northern Neuquén Precordillera (NNP). Location of Los Pábilos boulders (LP) and borehole geochronologic data of the Llanquihue Basement Complex (LBC) is shown with dotted lines (Hervé et al., 2016). Geochronologic constraints on the timing of metamorphism of the metamorphic basement of Argentina are also indicated (1: EPMA Th-U-Pb monazite, Urraza et al., 2008; 2: U-Pb titanite, Lucassen et al., 2004; 3: U-Pb titanite, Varela et al., 2005; and 4: EPMA Th-U-Pb monazite, Martínez et al., 2012).

In addition, no clear correlations have been so far established between the igneous-metamorphic basement of the North Patagonian Cordillera/massif and accretionary complexes exposed further west in Chile in terms of their structural and metamorphic evolution, though the latter record coeval Late Paleozoic sedimentation and subsequent deformation and metamorphism (Hervé et al., 2013; Kato et al., 2008; Martín et al., 1999; Willner et al., 2004). Recently, Hervé et al. (2016, 2018) identified juvenile Devonian magmatism in the accretionary complex of Chile south of 40°S and thus inferred the Late Devonian-Early Carboniferous accretion of an island arc complex along the southwestern margin of Gondwana. This hypothesis contrasts significantly with the proposal of Martínez et al. (2012), who suggested the collision of the Chilenia terrane at circa 390 Ma, well-documented north of 40°S (Willner et al., 2011).

On the other hand, a correct understanding of the coupling between deformation and metamorphism is critical for the reconstruction of P-T-D-t paths of deformed metamorphic rocks (Williams & Jercinovic,

2012) and their significance for orogenic evolution. In this sense, combined in situ petrologic and microstructural data allow to link deformation mechanisms, metamorphic reactions, and macroscopic structural features and to infer the relative timing of different mineral associations and microstructures (Goncalves et al., 2012; Hobbs et al., 2011; Johnson, 1999; Marsh et al., 2009; Oriolo et al., 2018; Skrzypek et al., 2011; Yakymchuk & Godin, 2012). The absolute timing of deformation and metamorphism, in turn, can be constrained by interpreting in situ geochronologic data in the light of microstructures, which provide insights into mineral equilibria, deformation mechanisms, and metamorphic reactions (Bosse & Villa, 2019; Gasser et al., 2015; Mulch & Cosca, 2004; Oriolo et al., 2016; Oriolo et al., 2018; Schulz, 2017; Tchato et al., 2009; Villa et al., 2014; Williams & Jercinovic, 2012). Furthermore, the integration of structural, microstructural, petrologic, and geochronologic data permits reconstructing the crustal architecture of orogens and contributes on the understanding of their tectonic and geodynamic evolution (e.g., Endo & Wallis, 2017; Goscombe & Gray, 2009; Raimondo et al., 2010).

In this contribution, new structural, microstructural, petrologic, and electron probe microanalysis (EPMA) Th-U-Pb monazite data from gneisses and schists of basement rocks of the North Patagonian Cordillera (southwestern Argentina) are shown, providing a reconstruction of the P-T-D-t path of the Gondwanide basement of the study area. Based on these results, a revised model for the tectonic evolution of northern Patagonia is presented, providing insights into the coupled evolution of the igneous-metamorphic basement of North Patagonian Cordillera/Massif and accretionary complexes of Chile, and the Late Paleozoic configuration of the southwestern Gondwana margin. In addition, geochronologic and structural constraints on the Mesozoic tectonic evolution of the North Patagonian Cordillera are included as well, based on the Jurassic-Cretaceous record of basement rocks.

## 2. Regional Setting

The North Patagonian Cordillera (southwestern Argentina) is located at the southern segment of the Central Andes and is bounded to the west and east by the Central Valley of Chile and the North Patagonian Massif, respectively (Figure 1). This morphostructural unit comprises an Andean thick-skinned fold and thrust belt and is essentially made up of Paleozoic igneous-metamorphic rocks, Mesozoic granitoids and subordinated volcano-sedimentary rocks, and Cenozoic volcano-sedimentary sequences and granites (Bechis, Encinas, et al., 2014; Castro, Moreno-Ventas, et al., 2011; Dalla Salda et al., 1991; Giacosa et al., 2001, 2005; Giacosa & Heredia, 2004; González Díaz, 1982; Iannelli et al., 2017; Rapela et al., 1988).

In the study area, located to the south of the Nahuel Huapi lake (Figure 2), the basement is considered to be part of the Colohuincul Complex (Dalla Salda et al., 1991) and comprises mostly paragneisses and schists with subordinated intercalations of amphibolites, metarhyolites, felsic orthogneisses, and foliated intrusions (Dalla Salda et al., 1991; García-Sansegundo et al., 2009). A structural characterization was presented by Dalla Salda et al. (1991) and García-Sansegundo et al. (2009), though quantitative structural data are still scarce. Martínez et al. (2012) obtained EPMA Th-U-Pb monazite ages of  $391.7 \pm 4.0$  and  $350.4 \pm 5.8$  Ma for migmatitic paragneisses near the Brazo Tronador, interpreted as the timing of peak and retrograde metamorphic conditions, respectively. For these rocks, metamorphic conditions of  $\sim 612$  °C and 4.9 kbar were determined. In addition, high-pressure metamorphism with peak conditions of  $\sim 440$  °C and 18 kbar was calculated for a garnet-bearing micaschist exposed at the southern margin of the Gutiérrez lake (Martínez et al., 2012). In this area, detrital zircons of metasedimentary rocks yield Early Paleozoic maximum sedimentation ages (Hervé et al., 2018).

Deformation and metamorphism of basement rocks of the North Patagonian Cordillera and the western North Patagonian Massif have been interpreted as the result of Late Paleozoic compression/transpression during the Gondwanide orogeny (García-Sansegundo et al., 2009; Giacosa et al., 2004; von Gosen, 2009). Within this framework, rocks of the study area were assigned to a hinterland position (García-Sansegundo et al., 2009). In contrast, Martínez et al. (2012) inferred a forearc setting for these rocks, associated with an older, Devonian collisional event, as recorded north of 40°S (Willner et al., 2011). The validity of this model was, however, questioned by Hervé et al. (2016, 2018). These authors proposed a Late Devonian-Early Carboniferous accretion of an island arc complex, considering igneous-metamorphic basement rocks of the North Patagonian Cordillera and the western North Patagonian Massif as remnants of a Devonian continental arc.

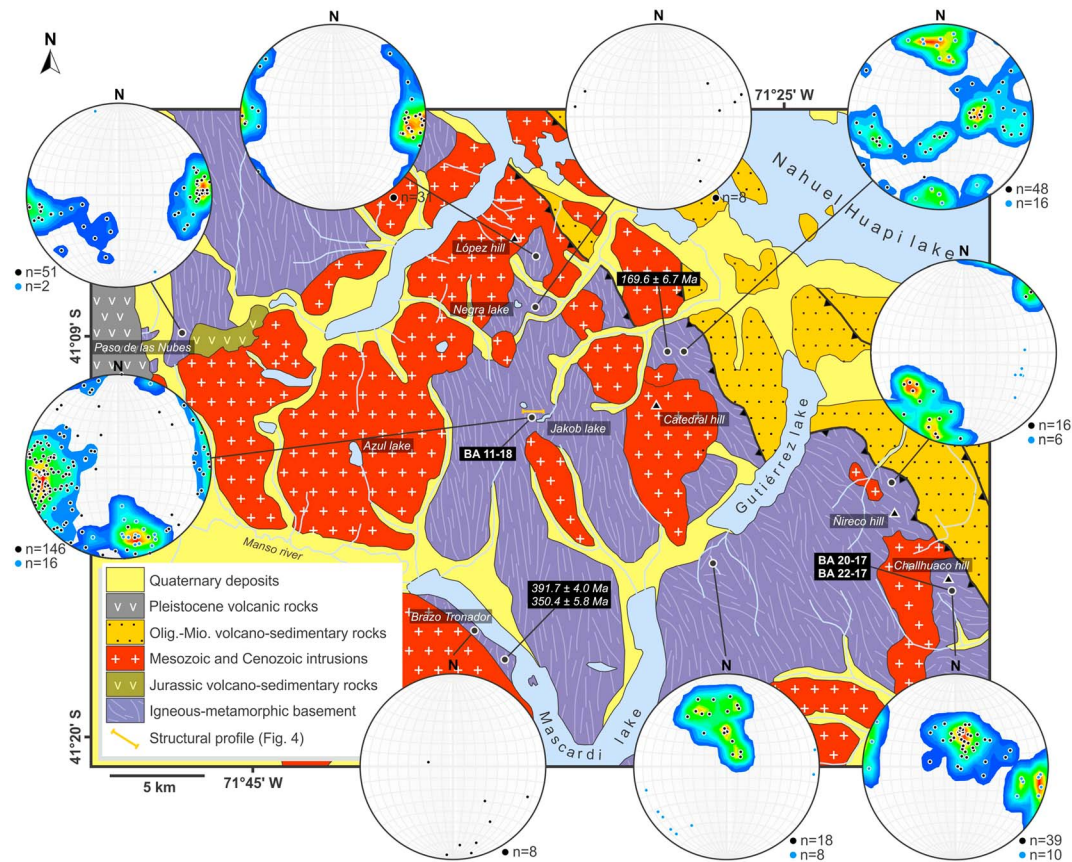


**Figure 2.** Geologic map of the study area (modified after Bechis, Cristallini, et al., 2014; Bechis, Encinas, et al., 2014; García-Sansegunado et al., 2009; González Bonorino, 1973; Greco, 1975). Monazite geochronologic data (italics) of Martínez et al. (2012) and sample locations (bold) are shown. Lower hemisphere equal area projections of poles of  $S_2$  (black dots) and  $L_2$  (blue dots) are also presented. Contour intervals at 2% per 1% area.

On the other hand, the Jurassic record of the study area is characterized by granitoids of the Cordilleran batholith yielding U-Pb SHRIMP zircon crystallization ages of circa 176–160 Ma (Castro, Moreno-Ventas, et al., 2011) and scarce volcano-sedimentary sequences (Giacosa et al., 2001). Based on pluton fabrics, Castro, Moreno-Ventas, et al. (2011) inferred regional sinistral strike-slip deformation, thus contrasting with the Middle-Late Jurassic extensional regime recorded by extensional structures of volcanic rock depocenters of the North Patagonian Cordillera located further south (Echaurren et al., 2016, 2017).

Finally, Cretaceous to Cenozoic rocks of the North Patagonian Cordillera are intimately related to Andean tectonics, with two main Middle-Late Cretaceous and Miocene orogenic phases (Gianni et al., 2018; Horton, 2018; Orts et al., 2012). In contrast to the Miocene transpressional phase, which is well recorded by structural, kinematic, and geochronologic data of volcano-sedimentary and granitic rocks (Bechis, Encinas, et al., 2014; Diraison et al., 1998; Giacosa et al., 2001, 2005; Giacosa & Heredia, 2004; Orts et al., 2012), the Cretaceous Andean record of the study area is only restricted to few granitoids yielding K-Ar and Rb-Sr ages of circa 120–80 Ma (González Díaz, 1982, and references therein). However, coeval thrusting was reported in adjacent regions of northwestern Patagonia (Echaurren et al., 2016, 2017; Gianni et al., 2018; Orts et al., 2012).

### 3. Methodology

Field mapping and structural analysis were applied in different exposures of the igneous-metamorphic basement of the North Patagonian Cordillera south of the Nahuel Huapi Lake (Figure 2), where samples were also collected for microstructural, geochronologic, and thermobarometric analysis. EPMA Th-U-Pb monazite data combined with SEM-based automated mineralogic methods were obtained in three samples of metasedimentary rocks (BA 20-17, BA 22-17, and BA 11-18). Sample descriptions and locations are

presented in Text S1 in the supporting information, whereas analytical details are provided in Text S2 in the supporting information. In addition, thermobarometry was applied in sample BA 22-17 in order to quantify pressure-temperature metamorphic conditions (Text S2 in the supporting information; Powell & Holland, 1994, 2008).

## 4. Results

### 4.1. Structure

The most conspicuous macroscopic fabric element is a metamorphic  $S_2$  foliation (Figure 2), though relics of bedding planes  $S_0$  and a metamorphic  $S_1$  foliation are occasionally observed as well (Figures 3a and 3b).  $S_1$  represents an axial plane foliation of isoclinal  $F_1$  folds affecting  $S_0$  planes, whereas  $S_2$  represents an axial plane foliation of tight to isoclinal  $F_2$  folds that fold  $S_1$  (Figure 3c), which is clearly observed at the microscale (see section 4.2). Rootless  $F_2$  hinges are common, being defined by folded quartz segregations, and in some cases,  $F_2$  folds are superimposed to isoclinal  $F_1$  folds (Figure 3d). The orientation of  $S_2$  planes is variable, despite showing a dominant NNW-SSE to WNW-ESE strike (Figure 3b). A stretching lineation  $L_2$  defined by shape-preferred orientation of micas and/or staurolite is associated with  $S_2$ , exhibiting subhorizontal plunges toward NNW-SSE to WNW-ESE, which is parallel to the strike of  $S_2$  planes in most cases (Figure 2).

Kink bands and late gentle to open  $F_3$  folds affecting  $S_2$  are also present exhibiting, in many cases, a kink geometry (Figures 3e and 3g). Though variable,  $F_3$  axial planes strike dominantly NE-SW and exhibit subvertical to steep dip toward SE. Fold hinge lines, in turn, show moderate plunge toward ENE and E. A spaced  $S_3$  foliation is occasionally observed as an axial plane foliation of  $F_3$ . On the other hand, a mylonitic  $S_3'$  foliation is also developed within low-grade shear zones (Figure 3f), comprising mostly ultramylonites, phylloinites, and pseudotachylites. Field relationships between kink bands and shear zones are not exposed. In some cases, a crenulation cleavage is associated with the mylonitic foliation, being localized within shear zone lozenges (Figure 3h), whereas a cataclastic overprint is observable as well.

The schematic structural profile of Figure 4 summarizes the relationship of different structural elements for the western margin of the Jakob lake (Figure 2). In this case,  $S_2$  planes strike dominantly NNW-SSE and dip steeply toward ENE, whereas  $L_2$  lineations plunge gently toward SSE. Tight to isoclinal  $F_2$  folds have subvertical hinge lines. Conjugated subvertical NE-SW and NW-SE striking kink bands exhibit subvertical axes. In a similar way, subvertical low-grade ductile to brittle-ductile  $S_3'$  shear zones strike dominantly NE-SW to NNE-SSW and show a dextral sense of shearing.

### 4.2. Microstructures

Schists are mostly made up of muscovite + biotite + quartz + plagioclase and characterized by the  $S_2$  foliation, which typically comprises a spaced schistosity. Schistosity domains are mostly made up of muscovite and subordinated biotite, whereas microlithons encompass quartz and, to a minor extent, plagioclase.  $S_2$  is commonly observed as a crenulation schistosity, due to the presence of relics of folded  $S_1$  planes in the microlithons of  $S_2$  (Figure 5a). In turn,  $S_1$  is characterized by muscovite + quartz + biotite  $\pm$  plagioclase. In addition, garnet and plagioclase porphyroblasts are frequently observed in the metapelitic schists (Figure 5b). Staurolite, K-feldspar, and sillimanite are occasionally present as well. Monazite, rutile, tourmaline, zircon, apatite, and titanite are accessory minerals.

Muscovite and biotite present shape-preferred orientation parallel to  $S_1$  and  $S_2$  planes, whereas quartz shows granoblastic microstructures and, in some cases, chessboard extinction (Figure 5c). Garnet and plagioclase porphyroblasts commonly exhibit inclusion trails defining folded  $S_1$  planes and strain shadows (muscovite + quartz + biotite + plagioclase  $\pm$  garnet) of  $S_2$  planes (Figures 5b and 5d), suggesting a syn- $S_2$  crystallization during folding (i.e.,  $F_2$ ) of  $S_1$ . Some syn- $S_2$  garnet porphyroblasts are also revealed by the presence of an internal rotated foliation that resembles  $S_2$  (Figure 5e). In a similar way, a syn- $S_2$  growth of plagioclase porphyroblasts is indicated by trails of inclusions that are parallel to  $S_2$  (Figure 5f).

Chlorite and fine-grained white mica are retrograde minerals replacing garnet, biotite, and plagioclase. Both minerals form fine-grained aggregates with shape-preferred orientation parallel to  $S_2$ , which is locally affected by mikrokinking or crenulation (Figure 5g; Text S1 in the supporting information). When present,  $S_3$  corresponds to a crenulation cleavage.

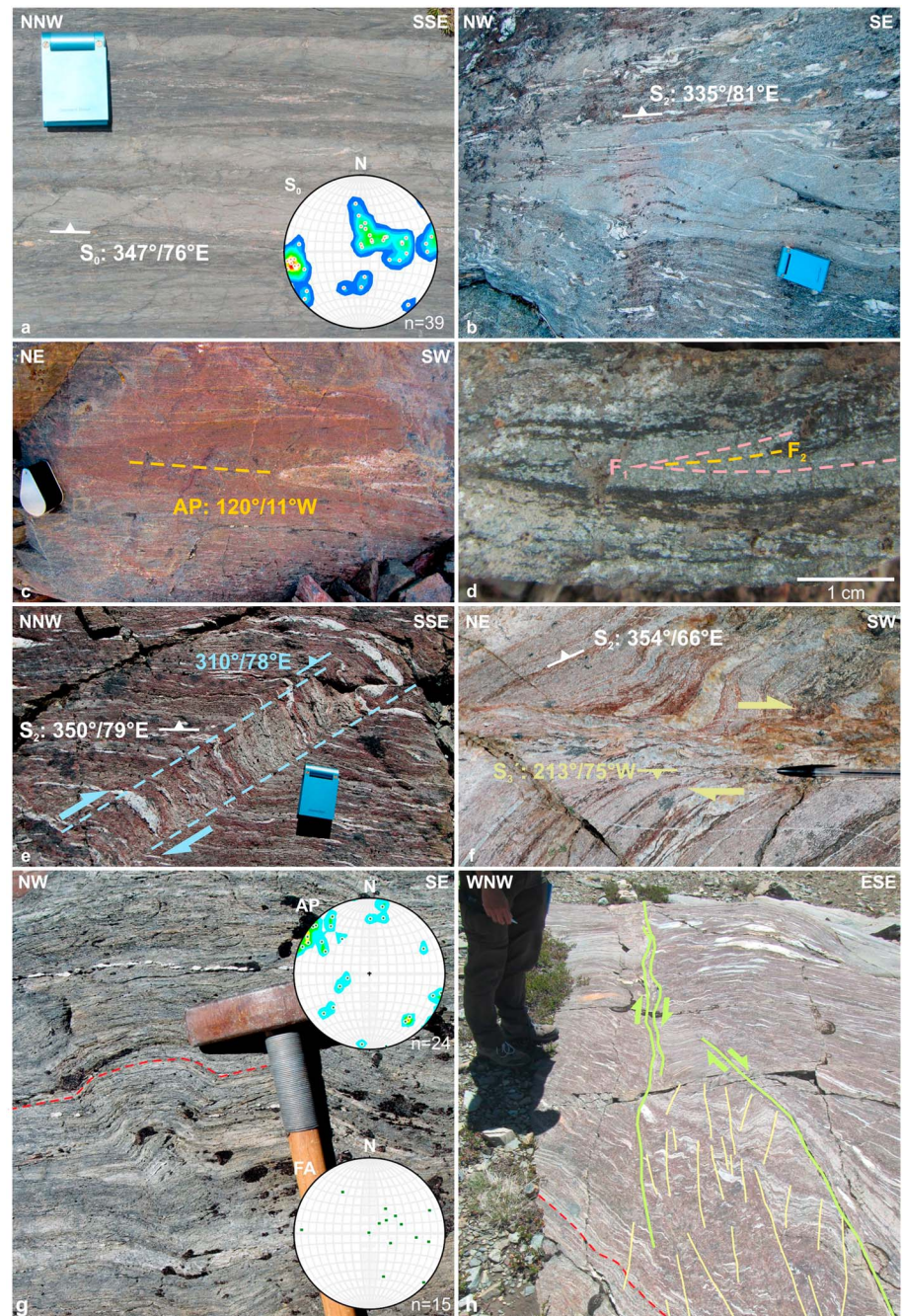


**Figure 3.** (a) Bedding planes ( $S_0$ ) defined by alternation of metapelites (dark gray) and metawackes (light gray). Lower hemisphere equal area projections of  $S_0$  poles. Contour intervals at 2% per 1% area. (b) NNW-SSE striking  $S_2$  foliation in paragneisses. (c) Axial plane (AP) of isoclinal  $F_2$  folds. (d) Axial plane traces of  $F_2$  folds overprinting  $F_1$  folds. (e) Dextral kink band cross-cutting  $S_2$  planes. (f) Mylonitic  $S_3'$  foliation in a dextral shear zone. (g) Example of  $F_3$  open kink fold. Lower hemisphere equal area projections of poles of  $F_3$  axial planes (AP) and axes (FA). Contour intervals at 2% per 1% area. Red line shows the orientation of the  $S_2$  foliation, whereas green lines indicate mylonitic  $S_3'$  foliation. (h) Development of crenulation cleavage (yellow lines) within a dextral shear zone lozenge, which corresponds to a contractional overstep (sensu Ponce et al., 2013). Red line shows the orientation of the  $S_2$  foliation, whereas green lines indicate mylonitic  $S_3'$  foliation.

Finally, ultramylonites and phyllonites of  $S_3'$  shear zones are made up of scarce porphyroclasts of plagioclase, muscovite, and opaque minerals immersed in a fine-grained matrix of quartz + chlorite + muscovite + biotite + opaque minerals. In the matrix, quartz is mostly restricted to granoblastic monomineralic layers, indicating postshearing recovery, whereas mica layers typically exhibit grain shape-preferred orientation

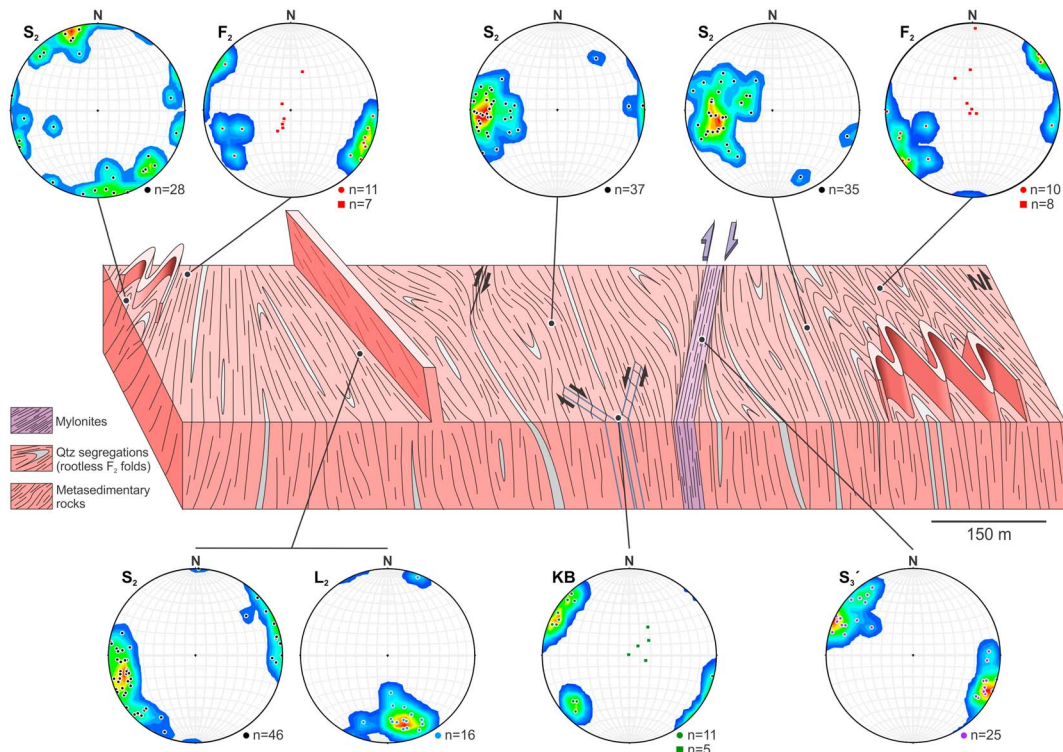


**Figure 4.** Schematic structural profile at the western margin of the Jakob lake. Lower hemisphere equal area projections of poles of different structural elements are also shown. Contour intervals at 2% per 1% area. In the case of  $F_2$  folds and kink bands (KB), circles and squares represent axial planes and axes, respectively. Rootless  $S_2$  folds defined by quartz (Qtz) segregations are schematically illustrated.

and local concentration of opaque minerals in trails parallel to the mylonitic foliation (Figure 5h), suggesting the role of dissolution-precipitation. Microstructures suggest that strain was mostly accommodated along mica-rich layers, with dissolution-precipitation as the main deformation mechanism, though subordinated bulging recrystallization was locally observed in quartz. However, evidence of cataclasis overprinting mylonitic features is common, with microfractures filled with fine-grained epidote + chlorite + white mica + quartz.

### 4.3. Mineral Chemistry and Thermobarometry

Garnet, white mica, biotite, plagioclase, and chlorite compositions in the garnet-bearing metapelite of sample BA 22-17 were determined. Analytic methods and results are provided in Text S1 and Table S1 in the supporting information, respectively.

Compositional zonation of garnets of up to 7-mm diameter was determined using the grain-based X-ray mapping (GXMAP) mode of automated scanning electron microscope (SEM) (Figure 6a). The garnet mineral chemical evolution was then detailed by EPMA analyses along profiles. In the porphyroblasts, the spessartine (Mn) contents decrease from ~9 to 1 mol % and the pyrope (Mg) contents increase from 3 to 11 mol % from core to rim, corresponding to a typical prograde zonation (Spear, 1993). The grossular (Ca) contents decrease from 28 to 10 mol %, whereas almandine increases from 60 to 77 mol %. In addition, a decrease of  $X_{Ca}$  from 0.27 to 0.05 and an increase of  $X_{Mg}$  from 0.03 to 0.14 are observed from cores to rims. Garnet outer rims display no significant increase of Mn and Ca. Unaltered biotite is rarely preserved in the micaschists and could be analyzed only when enclosed in plagioclase and quartz. According to their angular structural orientation in reference to the main foliation  $S_2$ , these biotites should be considered as  $S_1$  biotites. They have a  $X_{Mg}$  of ~ 0.46, with Ti of ~ 0.13 and  $^{IV}Al$  of ~ 0.18 (p.f.u.). Biotites in the main foliation  $S_2$  are mostly altered into chlorite, with totals below 92 wt %. Their  $X_{Mg}$  is ~ 0.52, with similar Ti and  $^{IV}Al$  as the  $S_1$  biotites. As biotite, the muscovite appears in the  $S_1$  microstructural position, mostly oblique to the main foliation  $S_2$ . Their  $Si^{4+}$  contents around 3.18 (p.f.u.) do not differ among different microstructural positions, similar to Na (~ 0.26–0.28 p.f.u.) and Mg (~ 0.06–0.08 p.f.u.) contents. On the other hand, chlorite appears in

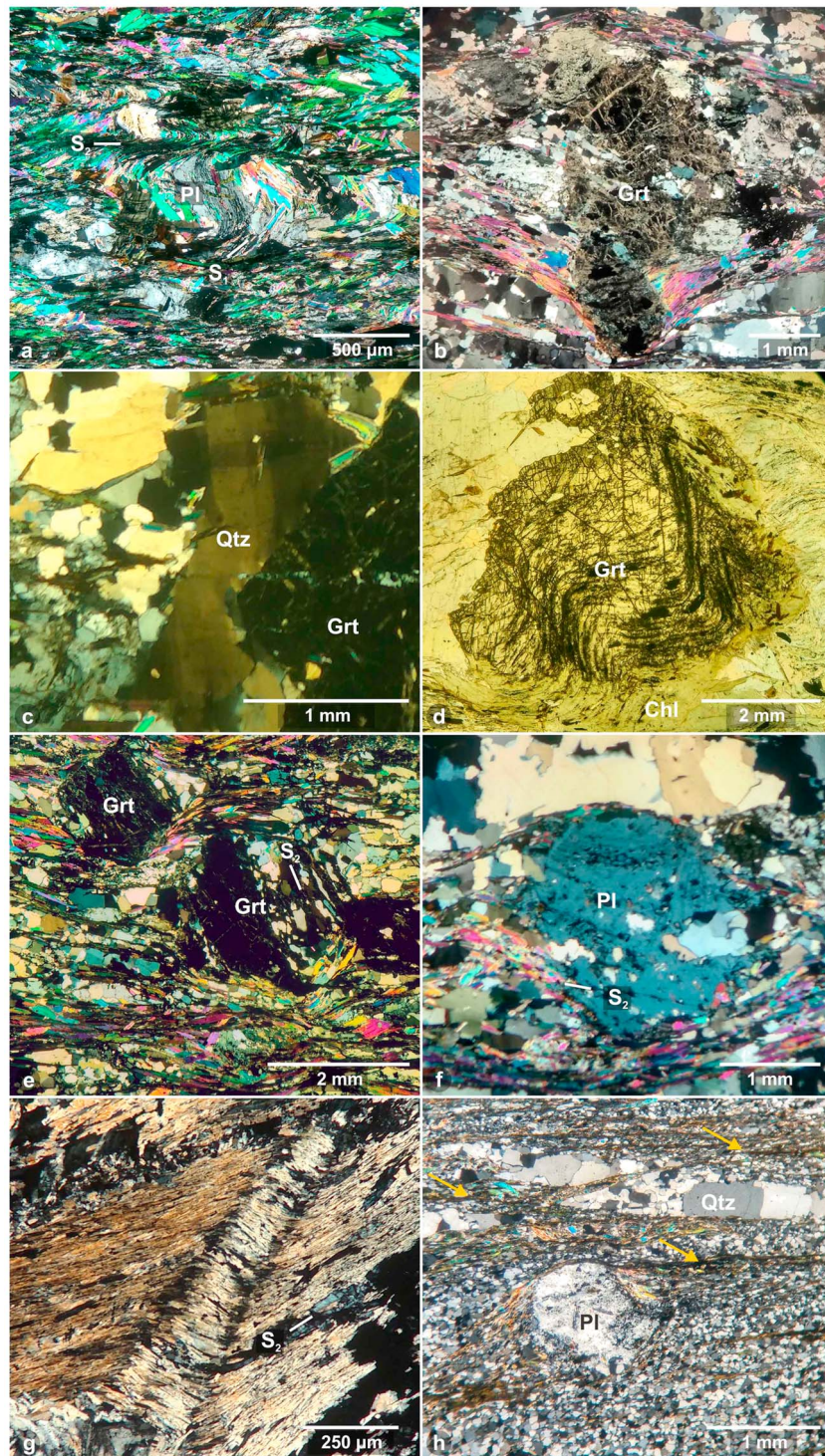


**Figure 5.** Photomicrographs of gneisses and schists of the study area. (a) Crenulation of  $S_1$  defined by inclusions of opaque minerals in plagioclase (Pl) and muscovite crystals (cross-polarized light).  $S_1$  is preserved within microlithons of the  $S_2$  crenulation schistosity. (b) Garnet (Grt) porphyroblast with  $S_2$  strain shadows (cross-polarized light). (c) Chessboard extinction in quartz (cross-polarized light). (d) Relics of  $S_1$  crenulation within a garnet porphyroblast, which shows chlorite replacement along rims (plain-polarized light). (e) Relics of rotated  $S_2$  foliation within garnet porphyroblasts (cross-polarized light). (f) Inclusion trails of opaque minerals within plagioclase porphyroblast that define an internal foliation, which is subparallel to  $S_2$  in the matrix (cross-polarized light). (g)  $S_2$  foliation replaced by retrograde white mica and chlorite and crosscut by microkink bands (cross-polarized light). (h) Ultramylonite showing plagioclase porphyroclast and monomineralic layers of granoblastic quartz in a fine-grained matrix (cross-polarized light). In the matrix, quartz is mostly granoblastic, whereas mica layers exhibit grain shape-preferred orientation and local concentration of opaque minerals in trails (yellow arrows) parallel to the mylonitic foliation.



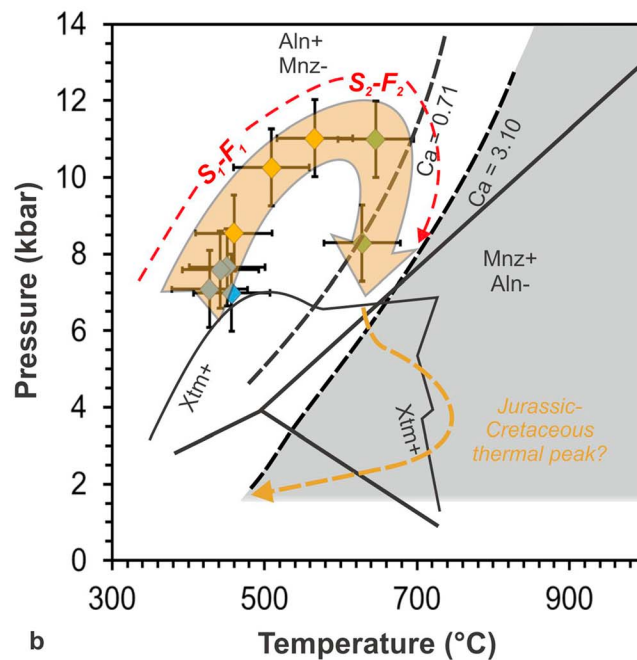
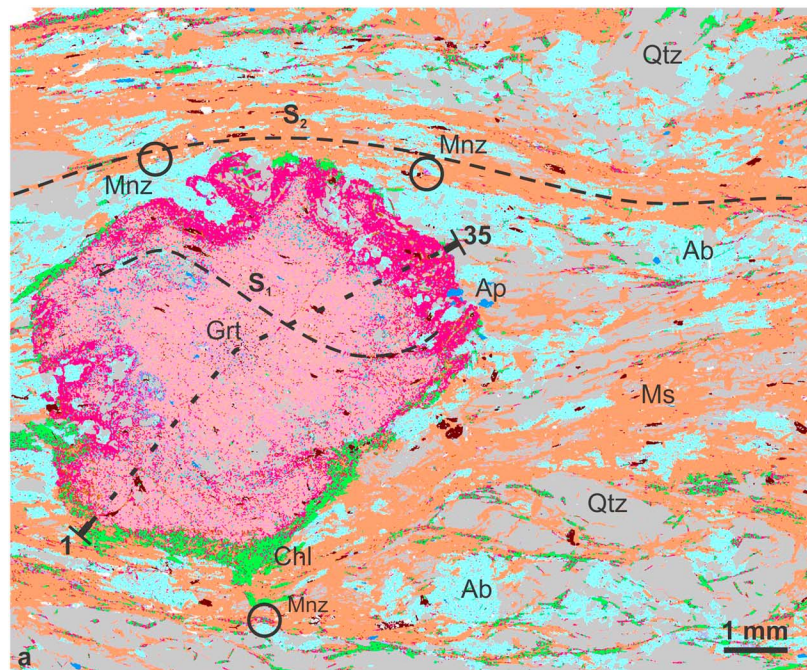


**Figure 6.** (a) Map of energy dispersive X-ray (EDX) spectra (GXMAP) of sample BA 22-17 from the Challhuaco hill. Spectra from zoned garnet (Grt) with variable Fe, Mg, Mn, and Ca contents in normalized element wt % are labeled with different colors. EDX spectra from muscovite (Ms), albite (Ab), chlorite (Chl), quartz (Qtz), and apatite (Ap) are also indicated by distinct colors. Locations of analytical profile (1 to 35) and traces of garnet internal foliation  $S_1$  and external foliation  $S_2$  are marked as well. Positions of some monazites along  $S_2$  are shown by circles. (b) P-T path of sample BA 22-17. Pressure estimations were obtained with the garnet-biotite-muscovite-plagioclase barometer (Wu, 2015), whereas temperature was calculated using garnet-biotite thermometer (Holdaway, 2000). Colors indicate garnet zonation (blue, core; yellow, middle; and green: rim). Stability fields of monazite and allanite at different bulk rock contents as a function of Ca molar content (dotted lines) are shown together with the xenotime stability field (Janots et al., 2007; Spear, 2010). Stability fields of  $Al_2SiO_5$  polymorphs are included as well. Mnz: monazite, Aln: allanite, Xtm: xenotime. Red arrows indicate the evolution of Carboniferous  $S_1-F_1$  to  $S_2-F_2$  fabrics related to the P-T path, whereas the brown arrow shows a schematic trajectory to explain Jurassic and Cretaceous monazite growth.

various microstructural positions (Text S1 in the supporting information). Along the margins of the garnet, replacement of garnet by chlorite is observed, with  $X_{Mg}$  of 0.52 at  $^{IV}Al$  of 2.58 and  $^{VI}Al$  of 2.75 (p.f.u.). Along  $S_2$  planes, the chlorite replaces the biotite at variable degrees, which led to  $X_{Mg}$  of 0.38–0.52,  $^{IV}Al$  of 2.23–2.58, and  $^{VI}Al$  of 2.73 (p.f.u.). Inclusions of plagioclase in the garnet porphyroblast are unzoned oligoclase and have anorthite contents between ~ 15 and 20 mol %. In the matrix along the foliation and next to the garnet margins, the small oligoclases are also unzoned but with lower anorthite contents between 11 and 15 mol %. Large plagioclase porphyroblasts in  $S_2$  microlithons, which enclose crenulated  $S_1$ , show the same variation in anorthite contents. In general, a trend toward slightly lower Ca contents during plagioclase crystallization can be defined.

The garnet crystallized with a low-variance assemblage of biotite, muscovite, plagioclase, and quartz. These phases occur as aligned inclusions in the garnet porphyroblasts, and also along  $S_1$  and  $S_2$  foliations. Rutile and ilmenite also occur in garnet porphyroblasts and in the foliated matrix. In terms of the garnet  $X_{Mg}$ - $X_{Ca}$  evolution (Spear, 1993), the garnet zonation semiquantitatively corresponds to a prograde metamorphism, with an initial increase of both pressure and temperature. The strong decrease of Ca toward the garnet rim signals subsequently decreasing pressure. Such a relative  $\Delta P/\Delta T$  trend appears to be mainly preserved when uncertainties about the corresponding plagioclase and biotite are considered (Spear, 1993).

Pressure and temperature for crystallization of garnet core were calculated by the calibrations of Holdaway (2000) and Wu (2015), involving enclosed plagioclase An17 and mica in the relic  $S_1$  foliation. This yielded ~ 400–450 °C at 7 kbar, with a slight dependency of the chosen biotite and plagioclase composition. A minimum error of  $\pm 50$  °C and  $\pm 1$  kbar has to be considered for each equilibrium calculation. Calculations for the middle parts of the garnet zonation profile with increased Mg contents, considering the composition of  $S_1$  biotites, led to higher temperatures and pressures. Peak conditions were calculated from garnet inner rims with 10 mol % grossular combined with matrix An15 plagioclase, yielding ~ 650 °C at 11 kbar (Figure 6b). A significant decrease of the grossular (Ca) content to 5 mol % toward the outer garnet rim resulted in a pressure drop to ~ 8 kbar for the final stage of the garnet crystallization during nearly isothermal conditions. The single P-T estimates from the zoned garnet define a clockwise P-T path within the kyanite stability field (Figure 6b). Alternative calculations with other thermobarometers and the avPT routine (Powell & Holland, 1994) yielded comparable results. After the P-T record of the garnet-bearing assemblage, a retrograde evolution with further decrease of pressure and temperature can be expected, as recorded by temperature of ~ 335 °C calculated from chlorite thermometry. As the P-T path enters the monazite stability field for low-Ca bulk rock compositions during decreasing pressure (Spear, 2010), monazites might start to grow at or shortly after peak conditions.

#### 4.4. Monazite Dating and Mineral Chemistry

In the case of garnet micaschists of the Challhuaco hill, a population of high-Th + U monazites in samples BA 20-17 and BA 22-17 yield nearly identical Late Pennsylvanian ages of  $299 \pm 8$  and  $302 \pm 16$  Ma, respectively (Figure 7). Likewise, sample BA 20-17 presents a low-Th + U monazite age population of  $80 \pm 20$  Ma, whereas a low-Th + U monazite age population of sample BA 22-17 exhibits an age of  $171 \pm 9$  Ma. The latter is comparable to the Middle Jurassic age recorded by sample BA 11-18, collected at the Jakob lake, which also yields a Cretaceous age of  $110 \pm 10$  Ma. Further analytic results are provided in Table S2 in the supporting information. Carboniferous monazites are typically large and almost lack in sutured grain boundaries. In contrast, Jurassic and Cretaceous monazites are smaller and show severely sutured grain boundaries and sponge-like microstructures, being also associated with fine-grained chlorite and white mica (Figure 7). The lack of Carboniferous monazites in sample BA 11-18 can be explained by the Ca bulk rock composition. The calculated values obtained from the automated SEM modal analysis of this sample indicate a considerably higher bulk rock Ca content (1.3 wt %) than samples BA 20-17 and BA 22-17 (0.7 and 0.52 wt %, respectively).

Monazite chemical composition supports a discrimination of age populations (Figure 8). Carboniferous monazites yield relatively homogeneous  $Y_2O_3$  contents, with most values between ~ 0.8 and 1.2 wt % (Figure 8a). In spite of their similar ages, Jurassic monazites of samples BA 22-17 and BA 11-18 show differences, with  $Y_2O_3$  contents that are lower or higher than a threshold value of ~ 1 wt %, respectively. The  $Y_2O_3$  content of Cretaceous monazites, in turn, varies between ~ 0.2 and 1.2 wt %. On the other hand, Carboniferous monazites present comparable  $X_{YPO_4}$  and  $X_{GdPO_4}$  contents between ~ 0.018 and 0.024

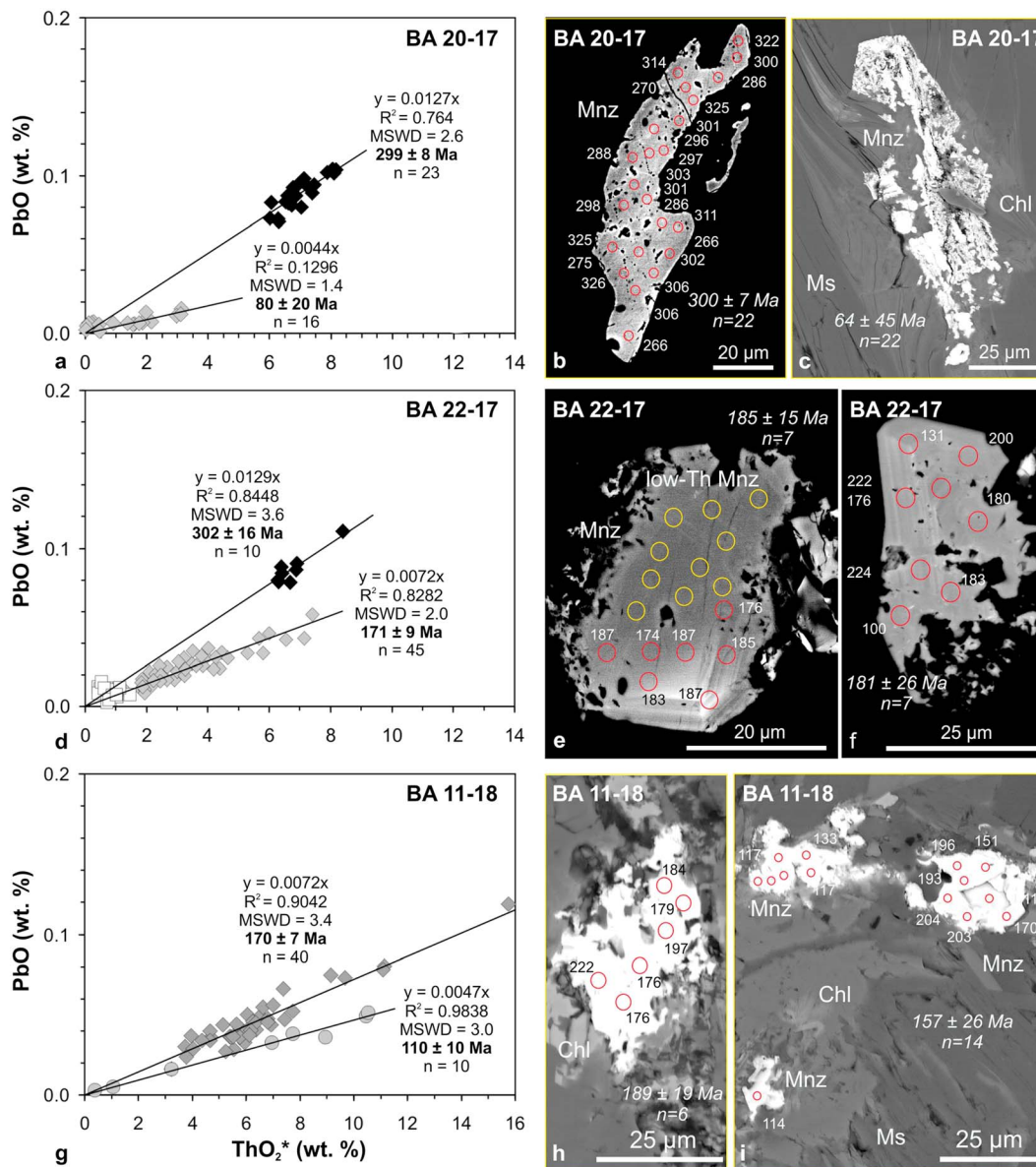


**Figure 7.** Th-U-Pb chemical model ages of monazite (a, d, g). Total  $\text{ThO}_2^*$  versus PbO (wt %) isochrones diagrams.  $\text{ThO}_2^*$  is  $\text{ThO}_2 + \text{UO}_2$  equivalents expressed as  $\text{ThO}_2$ . Regression lines with the coefficient of determination  $R^2$  are forced through zero (Montel et al., 1996; Suzuki et al., 1994). Weighted average ages (Ma) with MSWD and minimal  $2\sigma$  error are calculated from single analyses according to Ludwig (2001). The symbols mark analyses belong to distinct monazite age populations (circa 30–70 Ma, BA 20-17; circa 100–200 Ma, BA 11-18; circa 120–250 Ma, BA 22-18; and circa 280–330 Ma, BA 20-17 and BA 22-17) that define isochrones. White square symbols mark data of low-Th monazites, not considered for isochrone weighted mean ages. Backscattered electron images (BSE) of monazite (b, c, e, f, h, i), showing single Th-U-Pb ages (Ma) and weighted averages with  $2\sigma$  error calculated from several analyses within a grain. (a) BA 20-17, garnet micaschist, Challhuaco hill. (b) Monazite (Mnz) with Carboniferous ages. (c) Sponge-like monazite after strong alteration, situated in mica-rich domain with muscovite (Ms) and chlorite (Chl); weighted average age is calculated from low-Th analyses. (d) BA 20-17, garnet micaschist, Challhuaco hill. (e) Small monazite grain with low-Th contents in the upper part. Weighted average is calculated from lower part with 1–6 wt % Th. (f) Small Jurassic monazite with weak oscillatory zonation pattern. (g) BA 11-18, paragneiss, Jakob lake. (h) Strongly sutured monazite grain surrounded by chlorite. (i) Small and strongly sutured monazite grains with muscovite and chlorite. Only monazite with total > 98.5 wt % of oxides are considered for weighted average age.

(Figure 8b). All Jurassic monazites show  $X_{\text{GdPO}_4}$  contents higher than 0.016, though sample BA 11-18 shows  $X_{\text{YPO}_4}$  contents higher than those of sample BA 22-17.  $X_{\text{YPO}_4}$  and  $X_{\text{GdPO}_4}$  of the latter are relatively similar to those of Cretaceous monazites. Carboniferous and Jurassic monazites of sample BA 11-18 exhibit a positive correlation in the Th + U versus Ca plot, with Ca contents mostly higher than 0.1, as in the case of Cretaceous monazites (Figure 8c). In contrast, Jurassic monazites from sample BA 22-17 yield Ca contents

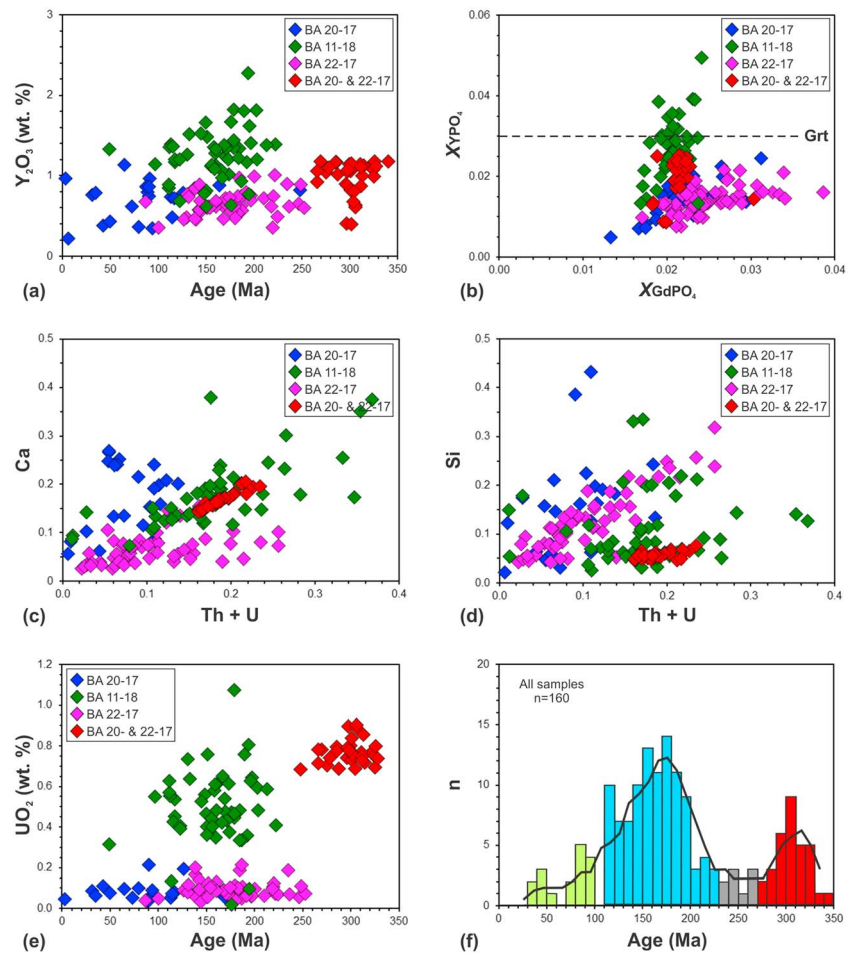


**Figure 8.** Mineral chemistry and distributions of monazite Th-U-Pb chemical ages (see also Figure 7). (a) Age versus Y<sub>2</sub>O<sub>3</sub>, showing elevated Y<sub>2</sub>O<sub>3</sub> contents in sample BA 11-18. (b) X<sub>GdPO<sub>4</sub></sub> versus X<sub>YPO<sub>4</sub></sub> (mole fractions). Maximum X<sub>YPO<sub>4</sub></sub> in garnet (Grt) mineral zone according to Pyle et al. (2001). (c) Th + U versus Ca (mole fractions). (d) Th + U versus Si (mole fractions). (e) Age versus UO<sub>2</sub>. (f) Histogram of monazite ages in all samples (BA 20-17, BA 22-17, and BA 11-18). Diverse distribution of Carboniferous, Jurassic, and minor Cretaceous monazite populations.

lower than 0.1. Both Carboniferous and Jurassic monazites of the Jakob lake show low Si contents (<0.15), whereas Cretaceous and Jurassic monazites of sample BA 22-17 exhibit values up to ~0.25 (Figure 8d). The latter also show a positive correlation between Th + U and Si. Carboniferous monazites show the highest UO<sub>2</sub> contents (>0.62%). Likewise, relatively high UO<sub>2</sub> contents are observed for Jurassic monazites of sample BA 11-18 (~0.24–0.8 wt %), thus showing a significant difference with low UO<sub>2</sub> contents of Cretaceous and Jurassic monazites of sample BA 22-17 (Figure 8e). In sum, Carboniferous and Jurassic ages are the most abundant groups in the monazite age distribution pattern, though a subordinated Cretaceous population is also well recorded (Figure 8f).

## 5. Discussion and Interpretation

### 5.1. P-T-D-t Path of the Gondwanide Basement

The ubiquitous S<sub>2</sub> foliation shows a dominant WNW-ESE to NNW-SSE strike (Figures 2 and 3), as reported by Dalla Salda et al. (1991) and García-Sansegundo et al. (2009). In a similar way, stretching lineations L<sub>2</sub> exhibit subhorizontal to gentle plunge to the NNW-SSE or WNW-ESE (Figures 2 and 4). Structural data point to bulk inclined transpression (Jones et al., 2004), with partitioning into strike-slip- and contraction-dominated domains suggested by differences in the orientation of S<sub>2</sub>, L<sub>2</sub>, and F<sub>2</sub> (Figures 2 and 4). Subvertical to steeply dipping S<sub>2</sub> and F<sub>2</sub> axial planes, steeply dipping F<sub>2</sub> hinges and gently plunging L<sub>2</sub>

lineations (e.g., Jakob lake and Paso de las Nubes) may record the former, whereas the latter may be registered by moderately to gently dipping  $S_2$  and  $F_2$  axial planes, and gently dipping  $F_2$  hinges subparallel to gently plunging  $L_2$  lineations (e.g., Ñireco and Challhuaco hills). Alternatively, such differences may arise from subsequent modifications due to Mesozoic and Cenozoic tectonic processes, which significantly overprinted the area (e.g., Bechis, Encinas, et al., 2014; Castro, Moreno-Ventas, et al., 2011; Giacosa & Heredia, 2004). Local variations are observed in the structural profile between the Témpanos and Jakob lakes (Figure 4), where significant post-Paleozoic deformation is absent. In the Paso de las Nubes area (Figure 2), on the other hand, the presence of Jurassic volcano-sedimentary rocks overlying the basement suggests the lack of post-Jurassic tilting, thus indicating a relative preservation of the orientation of basement fabrics (i.e., subvertical to steeply dipping  $S_2$  and subhorizontal to gently plunging  $L_2$ ), though vertical axis rotations cannot be discarded.

The garnet-bearing mineral assemblage of the Challhuaco hill schist records a first section of a prograde P-T path under conditions outside the monazite stability field, even for low bulk rock Ca compositions (Figure 6b). Crystallization of monazite can thus be expected at peak metamorphic conditions ( $\sim 650$  °C and 11 kbar) and mostly during subsequent decompression. In consequence, the Carboniferous monazite population will mark the minimum age for most of the prograde syn- $S_1$ - $S_2$  amphibolite facies event. Since monazites lie parallel to  $S_2$ , the timing of  $S_2$ - $L_2$  and associated  $F_2$  fabrics is constrained by EPMA Th-U-Pb monazite ages of  $299 \pm 8$  and  $302 \pm 16$  Ma (Figure 6), roughly coeval or slightly younger than peak metamorphic conditions of  $\sim 650$  °C and 11 kbar. Since  $S_1$  and  $S_2$  share structural and microstructural features (e.g., isoclinal folding), it can thus be inferred that  $S_1$ - $F_1$  may be Carboniferous in age as well. According to microstructural evidence (Figure 6a),  $S_1$ - $F_1$  may be related to prograde metamorphism developed prior to peak metamorphic conditions, being the evolution from  $S_1$ - $F_1$  to  $S_2$ - $F_2$  the result of progressive transpressional deformation (Carreras & Druguet, 2018; Fossen et al., 2018).

On the other hand, late deformation fabrics (i.e., kink bands,  $F_3$  open folds, shear zones) record low-grade metamorphic conditions. Kink bands and open folds are commonly associated with widespread crystallization of fine-grained chlorite and white mica (section 4.2, Text S1 in the supporting information; García-Sanseguno et al., 2009), for which mean temperature conditions of  $\sim 335$  °C were calculated from chlorite thermometry (section 4.3). In shear zones, mineral associations and microstructures suggest peak deformation conditions of  $\sim 350$ - $300$  °C, though evidence of late cataclasite and pseudotachylite development suggests further deformation below brittle-ductile transition conditions up to  $\sim 200$ - $150$  °C (Fagereng & Toy, 2011; Wallis et al., 2015; Wehrens et al., 2016). Despite being previously interpreted as the result of the final stages of the Gondwanide orogeny (García-Sanseguno et al., 2009), new evidence suggests a post-Paleozoic age for all these younger structures (see below). The pervasive crystallization of new monazite with low-Th + U contents during a wide time span during the Mesozoic suggests that associated deformation fabrics under retrograde metamorphic conditions might take place at considerably lower pressures than Carboniferous events (Figure 6b).

Comparison of P-T-D-t data obtained herein with previous P-T-t data from Martínez et al. (2012) suggests some differences among basement blocks in the study area in terms of P-T evolution and timing of metamorphism. Martínez et al. (2012) reported EPMA Th-U-Pb monazite ages of  $391.7 \pm 4.0$  and  $350.4 \pm 5.8$  Ma at the Brazo Tronador, for which metamorphic conditions of  $\sim 612$  °C and 4.9 kbar were determined. In addition, conditions of  $\sim 440$  °C and 18 kbar were determined for schists at the southern margin of the Gutiérrez lake (Martínez et al., 2012), but the timing of this high-pressure metamorphic event still remains elusive. Instead of a common P-T-D-t path (Dalla Salda et al., 1991; García-Sanseguno et al., 2009), basement blocks south of the Nahuel Huapi lake thus record different parts of a more complex long-term tectonometamorphic evolution, extending at least from circa 390 to 300 Ma (see also section 5.2). Hence, these rocks underwent not only deformation and metamorphism related to the Gondwanide orogeny, which is restricted to the Carboniferous-Permian (e.g., Heredia et al., 2017, 2018; Pankhurst et al., 2006), but also to pre-Gondwanide Devonian tectonometamorphic processes.

## 5.2. Implications for the Late Paleozoic Evolution of Northern Patagonia

Basement rocks exposed to the south of the Nahuel Huapi lake have been traditionally ascribed to the Colohuincul Complex (Dalla Salda et al., 1991; García-Sanseguno et al., 2009; Giacosa et al., 2001;

Martínez et al., 2012), which was defined by Turner (1965) to nucleate isolated outcrops of low-grade schists, quartzites, and phyllites exposed in the northernmost North Patagonian Cordillera and the Southern Neuquén Precordillera at  $\sim 39^\circ\text{S}$ . Both lithotypes and metamorphic grade in the *locus typicus* of the Colohuincul Complex contrast significantly with those of the study area (sections 2 and 4.3; García-Sanseguno et al., 2009; Martínez et al., 2012). In addition, metasedimentary rocks of the Colohuincul Complex were correlated with those of the Cushamen Formation (Cingolani et al., 2011, and references therein), which may have a late Carboniferous deposition age (Hervé et al., 2005; Marcos et al., 2018), being thus incompatible with Middle Devonian to Carboniferous ages of metamorphism reported for the study area (section 4.4; Martínez et al., 2012). For this reason, the Bariloche Complex is proposed as a new stratigraphic unit to include basement rocks exposed to the south of the Nahuel Huapi lake, which record Devonian-Carboniferous metamorphism and Early Paleozoic maximum deposition ages (Hervé et al., 2018).

On the other hand, EPMA Th-U-Pb monazite ages of circa 300 Ma (section 4.4) constrain the timing of deformation and metamorphism linked to the development of ubiquitous NNW-SSE to WNW-ESE striking  $S_2$  and associated  $L_2$  and  $F_2$  fabrics (section 5.1). Comparable NW-SE to NNW-SSE striking fabrics were also reported for medium-grade basement rocks of the western North Patagonian Massif, where foliated late Carboniferous intrusions occur as well (Cerrodo & López de Luchi, 1998; García-Sanseguno et al., 2009; Giacosa et al., 2004; Pankhurst et al., 2006; Renda et al., 2017; von Gosen, 2009). Furthermore, metasedimentary rocks recording Upper Devonian-Carboniferous low-grade metamorphism of the Northern and Southern Neuquén Precordillera (Figure 1) also exhibit NW-SE to NNW-SSE striking foliations (Franzese, 1993, 1995; Zappettini et al., 2012).

The timing of metamorphism and associated deformation of the basement in northwestern Patagonia is mostly constrained at circa 390–300 Ma (Figure 1), being thus comparable to the Devonian to Lower Permian ages of associated intrusions (Figure 9a; López de Luchi & Cerredo, 2008; Pankhurst et al., 2006; Varela et al., 2005). EPMA monazite ages of  $391.7 \pm 4.0$  and  $350.4 \pm 5.8$  Ma were obtained in migmatitic paragneisses near the Brazo Tronador (Martínez et al., 2012), whereas a U-Pb titanite age of  $380 \pm 2$  Ma was reported for a calc-silicate gneiss close to Piedra del Águila (Lucassen et al., 2004). Late Devonian metamorphism is evidenced by comparable ages of  $360 \pm 7$  (EPMA Th-U-Pb monazite, Urraza et al., 2008) and circa 359 Ma (U-Pb titanite data, Varela et al., 2005) reported further north in the North Patagonian Cordillera and Southern Neuquén Precordillera, respectively. In addition, Devonian to Carboniferous metamorphic overgrowths were reported in zircon grains from metasedimentary rocks at the Gutiérrez lake margin (Hervé et al., 2018) and El Maitén gneiss (Pankhurst et al., 2006), whereas whole-rock K-Ar ages of circa 380–300 Ma roughly constrain the timing of greenschist facies metamorphism of the Piedra Santa Complex in the Southern Neuquén Precordillera (Franzese, 1995).

Geochemical data of Devonian to Permian magmatic rocks spatially associated with basement inliers show a progressive increase of Sr/Y from the Devonian to the Lower Permian (Pankhurst et al., 2006; Varela et al., 2005, 2015), which may result from increasing crustal thickness (Figure 9a, Chapman et al., 2015; Chiaradia, 2015; Profeta et al., 2015). This is consistent with the crustal thickening event suggested by Cerredo and López de Luchi (1998) for this Late Paleozoic magmatism. P-T-t data of the basement show a similar trend, with younger ages of metamorphism for higher-pressure peak metamorphic conditions (sections 4 and 5.1, Martínez et al., 2012; Serra-Varela et al., 2017, 2018), although this trend could alternatively be explained by differential exhumation. Nevertheless, a progressive crustal thickening is further supported by the prograde P-T path of the Challhuaco sample (Figure 6). Peak P-T conditions and the relatively low geothermal gradient recorded during prograde metamorphism ( $\sim 10\text{--}20^\circ\text{C}/\text{km}$ , Figure 6) together with coeval intrusions at circa 330–300 Ma located immediately south (Pankhurst et al., 2006; Varela et al., 2005, 2015) suggest a position close to the arc-forearc transition in a Carboniferous continental arc setting for the Challhuaco schists (Figure 9b).

Ages of metamorphism recorded in accretionary complexes of Chile between circa 390–300 Ma are coeval with ages of metamorphism recorded in the metamorphic basement of the North Patagonian Cordillera and the western North Patagonian Massif (Figures 1 and 9a), accounting for a common evolution of all these areas, further supported by similarities in the orientation of NNW-SSE to WNW-ESE striking metamorphic foliations related to transpression (Figure 2, Martin et al., 1999; Duhart et al., 2001). In the high P/T Western Series at  $\sim 41^\circ\text{S}$  (Figure 1), a  $^{40}\text{Ar}/^{39}\text{Ar}$  hornblende plateau age of  $361.0 \pm 1.7$  Ma in a garnet-bearing

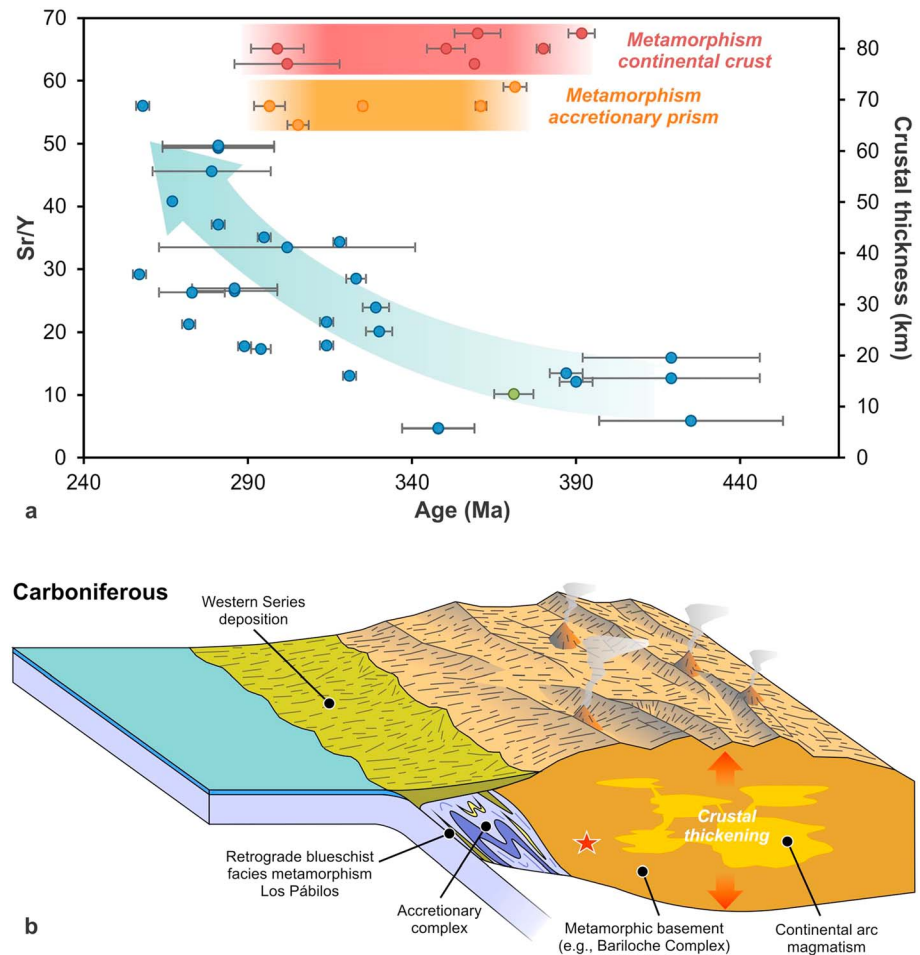


**Figure 9.** (a) Compilation of Sr/Y and U-Pb zircon geochronologic data (Pankhurst et al., 2006; Varela et al., 2005, 2015) of intrusions of Argentina (blue), recording increasing crustal thickness of the Late Paleozoic continental arc. Equivalent crustal thickness values were estimated using the equation of Chapman et al. (2015). Data from a granitic clast (green) of a conglomerate in Chile, which is inferred to derive from the Devonian continental arc in Argentina (Hervé et al., 2016; Quezada, 2015), are included as well. The timing of metamorphism of metamorphic complexes of Argentina (red; Lucassen et al., 2004; Varela et al., 2005; Urraza et al., 2008; Martínez et al., 2012; this work) and accretionary prism complexes of Chile (orange; McDonough *apud* Quezada, 2015; Kato et al., 2008; Willner et al., 2004) is also indicated. (b) Schematic Carboniferous tectonic setting for the region south of  $\sim 40^{\circ}\text{S}$  (modified after Kato et al., 2008; Martínez et al., 2012; Hervé et al., 2013, 2016). Continental arc magmatism is recorded by Carboniferous intrusions distributed between the North Patagonian Cordillera and the western North Patagonian Massif (Pankhurst et al., 2006; Varela et al., 2005, 2015). In the accretionary prism (Chile), deposition of the Western Series sedimentary protoliths takes place (Hervé et al., 2013), whereas the Los Pábilos boulders undergo exhumation and retrograde blueschist facies metamorphism (Kato et al., 2008; Willner et al., 2004). The red star shows the location of the Challhuaco hill samples. See section 5.2 for further details.

amphibolite of Los Pábilos boulders provides a minimum age for eclogite to epidote-amphibolite facies metamorphism at  $\sim 555^{\circ}\text{C}$  and  $> 13$  kbar (Kato et al., 2008), comparable to peak metamorphic conditions of  $\sim 600\text{--}760^{\circ}\text{C}$  and 11.0–16.5 kbar estimated by Willner et al. (2004) for these rocks. The age of subsequent retrograde blueschist facies metamorphism at circa  $350\text{--}500^{\circ}\text{C}$  and 10–14 kbar is constrained at  $305.3 \pm 3.2$  and  $296.6 \pm 4.7$  Ma by Rb-Sr mineral isochron data from garnet-bearing amphibolites and schists, respectively (Willner et al., 2004). A slightly older  $^{40}\text{Ar}/^{39}\text{Ar}$  muscovite age of  $325.0 \pm 1.1$  Ma was also reported for this event (Kato et al., 2008). On the other hand, K-Ar and  $^{40}\text{Ar}/^{39}\text{Ar}$  muscovite ages of circa 390–370 Ma from borehole samples of schists, further supported by an  $^{40}\text{Ar}/^{39}\text{Ar}$  hornblende inverse isochron age of  $359.3 \pm 4.4$  Ma of an undeformed granitic intrusion, indicate Devonian metamorphism for the Llanquihue Basement Complex (Figure 1, Hervé et al., 2016; McDonough *apud* Quezada, 2015).

The tectonometamorphic evolution of the Gondwanide basement and associated intrusions seem thus to record progressive crustal thickening related to a Late Paleozoic continental magmatic arc (Hervé et al., 2016; Varela et al., 2015). However, Martínez et al. (2012) suggested a Devonian collision of the Chilenia terrane as the most likely trigger for deformation and metamorphism of rocks of the North Patagonian Cordillera. This interpretation is based on the peak metamorphic conditions of  $\sim 440$  °C and 18 kbar calculated for a garnet-bearing micaschist exposed at the southern margin of the Gutiérrez lake and the EPMA Th-U-Pb monazite age of  $391.7 \pm 4.0$  Ma recorded by a migmatitic paragneiss of the Brazo Tronador. Since the latter also yielded peak metamorphic conditions of  $\sim 612$  °C and 4.9 kbar, the Devonian monazite age cannot be ascribed to high-P/low-T metamorphism but, instead, seem to be associated with low-P/high-T conditions. In contrast to the collisional model of Martínez et al. (2012), Hervé et al. (2016, 2018) proposed the Late Devonian-Early Carboniferous accretion of an island arc complex. Nevertheless, the proximity of the latter with respect to the continental arc (Hervé et al., 2018) makes the presence of two adjacent subduction zones unlikely. Alternatively, the development of a Carboniferous advancing accretionary orogen might be a likely trigger for the Gondwanide orogeny (Figure 9b), since it might increase the interplate coupling, thus leading to crustal thickening and a relative stabilization of the margin (e.g., Cawood et al., 2009). Therefore, the Gondwanide orogeny might be essentially linked to the evolution of a transpressional advancing orogen, developed along the continental margin of southwestern Gondwana.

### 5.3. The Basement Record of Mesozoic Tectonomagmatic Events

Monazite has a relatively high closure temperature for Pb diffusion, being  $>800$  °C for grain sizes larger than  $10 \mu\text{m}$  and cooling rates of  $10$  °C/my (Cherniak et al., 2004). Th diffusion is approximately 3 times slower than Pb diffusion (Cherniak & Pyle, 2008), and therefore, the Th-U-Pb system should remain closed in monazite under low-grade metamorphic conditions. Nevertheless, monazite commonly records low-grade metamorphic and hydrothermal events (e.g., Bergemann et al., 2017; Just et al., 2010; Oyhantçabal et al., 2012; Poitrasson et al., 1996; Teufel & Heinrich, 1997). Such disturbances of the Th-U-Pb system seem to arise from mechanisms, such as neocrystallization, recrystallization, and dissolution/reprecipitation, instead from diffusive exchange (Cherniak et al., 2004; Cherniak & Pyle, 2008; Gardés et al., 2006; Harlov et al., 2011; Kelsey et al., 2008; Oriolo et al., 2018).

Though Jurassic magmatism is widespread in the North Patagonian Cordillera (Castro, Moreno-Ventas, et al., 2011; Echaurren et al., 2017), evidence of coeval metamorphism and associated deformation is still scarce. In the study area, the igneous-metamorphic basement hosts the Jurassic Cordilleran batholith, which yields U-Pb SHRIMP zircon crystallization ages of circa 176–160 Ma (Castro, Moreno-Ventas, et al., 2011). The only Jurassic record reported so far for basement rocks is a EPMA Th-U-Pb monazite age of  $169.6 \pm 6.7$  Ma for a micaschist of the Catedral hill, which was attributed to contact metamorphism caused by Jurassic magmatism (Martínez et al., 2012), possibly related to a close tonalitic intrusion. Interestingly, monazite data (section 4.4) record comparable Middle Jurassic ages of  $171 \pm 9$  and  $170 \pm 7$  Ma. Microstructural evidence shows that Jurassic monazites are spatially associated with retrograde micas, which show shape-preferred orientation parallel to  $S_2$  and are affected by  $F_3$  microfolds and microkink bands (Figures 5f and 7). Therefore, monazite ages are interpreted to record the timing of Jurassic low-grade metamorphism and deformation constrained at  $\sim 335$  °C by chlorite thermometry. Though Jurassic granitoids are absent in the Jurassic sample locations, the influence of magmatism in these ages cannot be discarded.

The here obtained monazite ages are similar to the U-Pb SHRIMP zircon age of  $175.9 \pm 4.9$  Ma reported for a granulite xenolith enclosed in Paleogene basalts to the south of the North Patagonian Massif (Castro, Aragón, et al., 2011), whereas slightly older Early Jurassic intraplate deformation was documented by K-Ar and Ar/Ar mica data of Paleozoic granitoids in the northeastern North Patagonian Massif (Martínez Dopico et al., 2017). Recently, extension-related very low-grade metamorphism was recognized in the Southern and Northern Neuquén Precordillera (Suárez & González, 2018). Further evidence suggesting a Jurassic age for low-grade metamorphism and deformation is provided by late deformation fabrics, so far considered to be related to the Gondwanide orogeny (García-Sansegundo et al., 2009). Sample BA 11-18 was collected close to conjugated kink bands (Figure 4), which are also microscopically observed (Figure 5f and Text S1 in the supporting information). Considering the orientation and kinematics of both sets of kink bands (e.g., Carreras et al., 2013; Cobbold et al., 1971), a NNW-SSE shortening direction (present coordinates) can be inferred, further supported by magmatic fabrics of Jurassic plutons (Castro, Moreno-



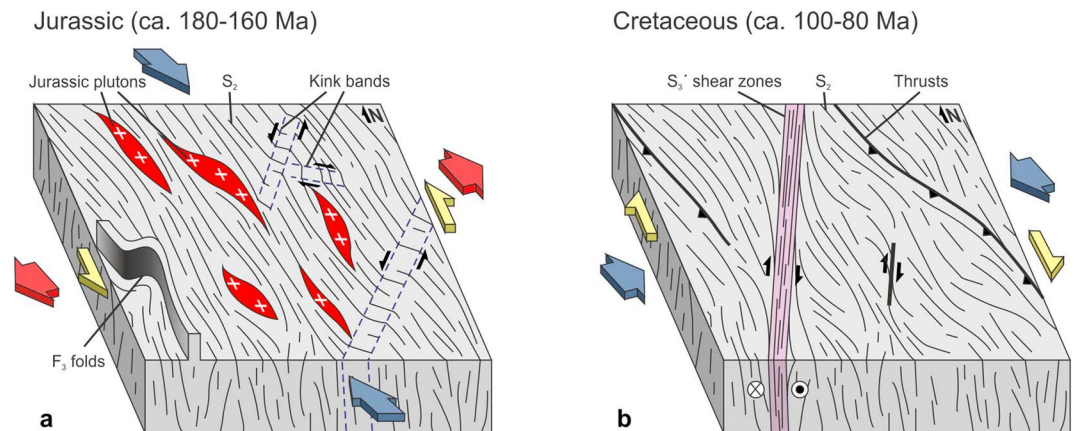


**Figure 10.** Schematic Jurassic (a) and Cretaceous (b) structural evolution of the study area. Maximum shortening (blue arrows) and extension (red arrows) directions together with strike-slip component (yellow arrows) are indicated. See section 5.3 for further details. (a) Emplacement of Jurassic magmatism and development of conjugated kink bands and  $F_3$  open folds in a strike-slip-dominated transtensional setting (modified after Castro, Moreno-Ventas, et al., 2011). (b) Thrusting and dextral shearing related to dextral transpression.

Ventas, et al., 2011). Comparable sets of conjugated brittle structures related to Jurassic deformation were reported to the southeast in the Deseado Massif (Japas et al., 2013; Reimer et al., 1996). Likewise, Jurassic volcanism, ore deposits, and sedimentation recorded elsewhere in Patagonia have been mostly attributed to NE-SW to ENE-WSW extension and NW-SE to NNW-SSE shortening (Bechis, Cristallini, et al., 2014; Giacosa et al., 2010; Japas et al., 2017; Naipauer et al., 2012; Navarrete et al., 2016, 2018; Páez et al., 2011; Pankhurst et al., 2000; Silvestro & Zubiri, 2008; Rapela et al., 2005).

Considering the NNW to NW convergence direction along the proto-Andean paleo-Pacific margin determined for the circa 180–160 Ma period (Müller et al., 2016) and all aforementioned structural evidence, a regional strike-slip-dominated transtensional regime can thus be inferred for Patagonia in the Jurassic (Figure 10a; e.g., Giacosa et al., 2010; Castro, Moreno-Ventas, et al., 2011; Japas et al., 2013). In such a setting, both kink bands and  $F_3$  open folds can be explained (section 4.1 and Figure 10a; Fossen et al., 2013). Besides, the extensional component might favor the development of a thermal anomaly, leading to a relatively high geothermal gradient (Castro, Aragón, et al., 2011; Suárez & González, 2018) that may explain the obtained monazite ages (Figure 6b).

Cretaceous monazite ages of  $110 \pm 10$  and  $80 \pm 20$  Ma are associated with randomly oriented fine-grained aggregates of chlorite + white mica + opaque minerals  $\pm$  epidote, which in some cases are located along microveins. In this context, monazite ages seem to record the timing of hydrothermal activity, possibly related to Cretaceous granitoids in the North Patagonian Cordillera suggested by K-Ar and Rb-Sr ages of circa 120–80 Ma (González Díaz, 1982, and references therein).

On the other hand, dextral NE-SW to NNE-SSW striking subvertical  $S_3'$  shear zones are comparable in terms of orientation and kinematics to dextral NE-SW to NNE-SSW striking subvertical faults related to Andean Neogene transpression in the North Patagonian Cordillera (Diraison et al., 1998). However, deformation conditions estimated for shear zones (sections 4.2 and 5.1) indicate that they underwent deformation in a deeper crustal level than Neogene faults, and therefore, a more likely Cretaceous age is inferred for shear zones. This is further supported by middle Cretaceous deformation associated with ENE-NE shortening directions documented in northwestern Patagonia, where coeval tectonic activity along NNW-SSE to NNE-SSW striking thrusts was also reported (Echaurren et al., 2016, 2017; Gianni et al., 2018; Orts et al., 2012). Hence, shear zones might result from an early Andean Cretaceous dextral transpressional event (Figure 10b), probably associated with coeval magmatism and hydrothermal events recorded by monazite ages, as the latter match the onset of Andean tectonics at circa 100–95 Ma (Somoza & Zafaranna, 2008). Nevertheless, further geologic, geochronologic, and structural data are still necessary to assess the evolution of Cretaceous tectonomagmatic and hydrothermal processes.

## 6. Conclusions

Combined field structural data with in situ EPMA Th-U-Pb monazite, petrologic, and microstructural data allow reconstructing the P-T-D-t path of the Gondwanide basement of the North Patagonian Cordillera. For samples from the Challhuaco hill, the timing of development of the metamorphic  $S_2$  foliation and associated  $L_2$  lineations and  $F_2$  folds is constrained by monazite ages of  $299 \pm 8$  and  $302 \pm 16$  Ma during or shortly after peak metamorphic conditions of  $\sim 650$  °C and 11 kbar, whereas  $S_1$ - $F_1$  fabrics might be related to prograde metamorphism developed prior to these peak conditions. Within this framework, the evolution from  $S_1$ - $F_1$  to  $S_2$ - $F_2$  seems to be the result of progressive transpressional deformation.

The prograde P-T path recorded by samples of the Challhuaco hill together with regional evidence suggests Late Paleozoic crustal thickening. Contemporaneous metamorphism and deformation recorded by metamorphic complexes of northwestern Patagonia (Argentina) and accretionary complexes exposed further west (Chile) point to a common evolution of both areas, most likely resulting from Carboniferous transpression due to advancing subduction. Instead of the result of collision of large continental blocks, the Gondwanide orogeny might thus be essentially linked to geodynamic processes associated with subduction along the proto-Pacific margin of Gondwana.

On the other hand, monazite ages of  $171 \pm 9$  and  $170 \pm 7$  Ma indicate a Middle Jurassic low-grade metamorphic overprint coeval with development of kink bands and  $F_3$  open folds. This Middle Jurassic deformation event was contemporaneous with the emplacement of Cordilleran granitoids in the North Patagonian Cordillera and might result from a regional transtensional event, ubiquitously recorded in Patagonia. Finally, monazite ages of  $110 \pm 10$  and  $80 \pm 20$  Ma are interpreted to result from hydrothermal processes, possibly related to Cretaceous magmatism. The timing of deformation along low-grade dextral NE-SW to NNE-SSW striking subvertical shear zones seems to be coeval, thus recording middle Cretaceous dextral transpression associated with the onset of Andean tectonics.

### Acknowledgments

Sebastián Oriolo thanks financial support of the National Geographic Society (grant CP-123R-17) and Agencia Nacional de Promoción Científica y Tecnológica (PICT-2017-1092). Support at the SEM studies in the Laboratory of Geometallurgy at Freiberg was provided by S. Gilbricht. Pablo González thanks financial support of the Universidad Nacional de Río Negro (PI-UNRN-40-A-462) and Agencia Nacional de Promoción Científica y Tecnológica (PICT-2015-0787), whereas Florencia Bechis acknowledges financial support of the Agencia Nacional de Promoción Científica y Tecnológica (PICT-2010-2240 and PICT-2017-3259). The authors also wish to thank the administration of the Parque Nacional Nahuel Huapi for allowing field work in the area. Mariano Sebesta and all people from the Refugio Agostino Rocca and Refugio López are greatly acknowledged for their hospitality during the fieldwork. John Geissman is thanked for the editorial handling and Djordje Grujić, Pedro Castiñeiras, and Werner von Gosen for their critical comments, which significantly contributed to improve the manuscript. All data used in the manuscript are available in the text, figures, and supporting information (Texts S1 and S2, and Tables S1 and S2). In the case of previously published data, data are referred to their sources, which are listed in the References.

### References

- Bechis, F., Cristallini, E. O., Giambiagi, L. B., Yagupsky, D. L., Guzmán, C. G., & García, V. H. (2014). Transtensional tectonics induced by oblique reactivation of previous lithospheric anisotropies during the Late Triassic to Early Jurassic rifting in the Neuquén basin: Insights from analog models. *Journal of Geodynamics*, 79, 1–17. <https://doi.org/10.1016/j.jog.2014.04.010>
- Bechis, F., Encinas, A., Concheyro, A., Litvak, V. D., Aguirre-Urreta, B., & Ramos, V. A. (2014). New age constraints for the Cenozoic marine transgressions of northwestern Patagonia, Argentina ( $41^\circ$ – $43^\circ$  S): Paleogeographic and tectonic implications. *Journal of South American Earth Sciences*, 52, 72–93. <https://doi.org/10.1016/j.jsames.2014.02.003>
- Bergemann, C., Gnos, E., Berger, A., Whitehouse, M., Mullis, J., Wehrens, P., et al. (2017). Th-Pb ion probe dating of zoned hydrothermal monazite and its implications for repeated shear zone activity: An example from the Central Alps, Switzerland. *Tectonics*, 36, 671–689. <https://doi.org/10.1002/2016TC004407>
- Bosse, V., & Villa, I. M. (2019). Petrochronology and hydrochronology of tectono-metamorphic events. *Gondwana Research*, 71, 76–90. <https://doi.org/10.1016/j.gr.2018.12.014>
- Carreras, J., Cosgrove, J. W., & Druguet, E. (2013). Strain partitioning in banded and/or anisotropic rocks: Implications for inferring tectonic regimes. *Journal of Structural Geology*, 50, 7–21. <https://doi.org/10.1016/j.jsg.2012.12.003>
- Carreras, J., & Druguet, E. (2018). Complex fold patterns developed by progressive deformation. *Journal of Structural Geology*, 125, 195–201. <https://doi.org/10.1016/j.jsg.2018.07.015>
- Castillo, P., Fanning, C. M., Pankhurst, R. J., Hervé, F., & Rapela, C. W. (2017). Zircon O- and Hf-isotope constraints on the genesis and tectonic significance of Permian magmatism in Patagonia. *Journal of the Geological Society*, 174(5), 803–816. <https://doi.org/10.1144/jgs2016-152>
- Castro, A., Aragón, E., Díaz-Alvarado, J., Blanco, I., García-Casco, A., Vogt, K., & Liu, D. -Y. (2011). Age and composition of granulite xenoliths from Paso de Indios, Chubut province, Argentina. *Journal of South American Earth Sciences*, 32(4), 567–574. <https://doi.org/10.1016/j.jsames.2011.06.001>
- Castro, A., Moreno-Ventas, I., Fernández, C., Vujovich, G., Gallastegui, G., Heredia, N., et al. (2011). Petrology and SHRIMP U-Pb zircon geochronology of Cordilleran granitoids of the Bariloche area, Argentina. *Journal of South American Earth Sciences*, 32(4), 508–530. <https://doi.org/10.1016/j.jsames.2011.03.011>
- Cawood, P. A., Kröner, A., Collins, W. J., Kusky, T. M., Mooney, W. D., & Windley, B. F. (2009). Accretionary orogens through Earth history. In P. A. Cawood, & A. Kröner (Eds.), *Earth accretionary systems in space and time* (Vol. 318, pp. 1–36). London: Geological Society of London.
- Cerrodo, M. E., & López de Luchi, M. G. (1998). Mamil Choique Granitoids, southwestern North Patagonian Massif, Argentina: Magmatism and metamorphism associated with a polyphasic evolution. *Journal of South American Earth Sciences*, 11(5), 499–515. [https://doi.org/10.1016/S0895-9811\(98\)00025-X](https://doi.org/10.1016/S0895-9811(98)00025-X)
- Chapman, J. B., Ducea, M. N., DeCelles, P. G., & Profeta, L. (2015). Tracking changes in crustal thickness during orogenic evolution with Sr/Y: An example from the North American Cordillera. *Geology*, 43(10), 919–922. <https://doi.org/10.1130/G36996.1>
- Cherniak, D. J., & Pyle, J. M. (2008). Th diffusion in monazite. *Chemical Geology*, 256(1–2), 52–61. <https://doi.org/10.1016/j.chemgeo.2008.07.024>
- Cherniak, D. J., Watson, E. B., Grove, M., & Harrison, T. M. (2004). Pb diffusion in monazite: A combined RBS/SIMS study. *Geochimica et Cosmochimica Acta*, 68(4), 829–840. <https://doi.org/10.1016/j.gca.2003.07.012>

- Chiaradia, M. (2015). Crustal thickness control on Sr/Y signatures of recent arc magmas: An Earth scale perspective. *Scientific Reports*, 5(1), 8115. <https://doi.org/10.1038/srep08115>
- Cingolani, C. A., Zanettini, J. C. M., & Leanza, H. A. (2011). El basamento ígneo y metamórfico. In H. A. Leanza, C. Arregui, O. Carbone, J. C. Danieli, & J. M. Vallés (Eds.), *Relatorio del XVIII Congreso Geológico Argentino*, (pp. 37–47). Neuquén: Asociación Geológica Argentina.
- Cobbold, P. R., Cosgrove, J. W., & Summers, J. M. (1971). Development of internal structures in deformed anisotropic rocks. *Tectonophysics*, 12(1), 23–53. [https://doi.org/10.1016/0040-1951\(71\)90065-5](https://doi.org/10.1016/0040-1951(71)90065-5)
- Dalla Salda, L. H., Cingolani, C. A., & Varela, R. (1991). El basamento cristalino de la región norpatagónica de los lagos Gutiérrez, Mascardi y Guillermo, provincia de Río Negro. *Revista de la Asociación Geológica Argentina*, 46(3-4), 263–276.
- Dalla Salda, L. H., Dalziel, I. W. D., Cingolani, C. A., & Varela, R. (1992). Did the Taconic Appalachians continue into southern South America? *Geology*, 20(12), 1059–1062. [https://doi.org/10.1130/0091-7613\(1992\)020<1059:DTTACI>2.3.CO;2](https://doi.org/10.1130/0091-7613(1992)020<1059:DTTACI>2.3.CO;2)
- Diraison, M., Cobbold, P. R., Rossello, E. A., & Amos, A. J. (1998). Neogene dextral transpression due to oblique convergence across the Andes of northwestern Patagonia, Argentina. *Journal of South American Earth Sciences*, 11(6), 519–532. [https://doi.org/10.1016/S0895-9811\(98\)00032-7](https://doi.org/10.1016/S0895-9811(98)00032-7)
- Duhart, P., McDonough, M., Muñoz, J., Martin, M., & Villeneuve, M. (2001). El Complejo Metamórfico Bahía Mansa en la cordillera de la Costa (39°30'–42°00'S): Geocronología K-Ar, <sup>40</sup>Ar/<sup>39</sup>Ar y U-Pb e implicancias en la evolución del margen sur-occidental de Gondwana. *Revista Geológica de Chile*, 28(2), 179–208.
- Echaurren, A., Folguera, A., Gianni, G., Orts, D., Tassara, A., Encinas, A., et al. (2016). Tectonic evolution of the North Patagonian Andes (41°–44° S) through recognition of syntectonic strata. *Tectonophysics*, 677–678, 99–114. <https://doi.org/10.1016/j.tecto.2016.04.009>
- Echaurren, A., Oliveros, V., Folguera, A., Ibarra, F., Creixell, C., & Lucassen, F. (2017). Early Andean tectonomagmatic stages in north Patagonia: Insights from field and geochemical data. *Journal of the Geological Society*, 174(3), 405–421. <https://doi.org/10.1144/jgs2016-087>
- Endo, S., & Wallis, S. R. (2017). Structural architecture and low-grade metamorphism of the Mikabu-Northern Chichibu accretionary wedge, SW Japan. *Journal of Metamorphic Geology*, 35(6), 695–716. <https://doi.org/10.1111/jmg.12251>
- Fagereng, Å., & Toy, V. G. (2011). Geology of the earthquake source: An introduction. In Å. Fagereng, V. G. Toy, & J. V. Rowland (Eds.), *Geology of the earthquake source: A volume in honour of Rick Sibson*, (Vol. 359, pp. 1–16). London: Geological Society of London.
- Fossen, H., Cavalcante, G. C. G., Pinheiro, R. V. L., & Archanjo, C. J. (2018). Deformation—Progressive or multiphase? *Journal of Structural Geology*, 125, 82–99. <https://doi.org/10.1016/j.jsg.2018.05.006>
- Fossen, H., Teyssier, C., & Whitney, D. L. (2013). Transtensional folding. *Journal of Structural Geology*, 56, 89–102. <https://doi.org/10.1016/j.jsg.2013.09.004>
- Franzese, J. R. (1993). Deformación preandina del basamento del Cordón de la Piedra Santa, Neuquén. Paper presented at the XII Congreso Geológico Argentino, Mendoza, Argentina.
- Franzese, J. R. (1995). El Complejo Piedra Santa (Neuquén, Argentina): Parte de un cinturón metamórfico neopaleozoico del Gondwana suroccidental. *Revista Geológica de Chile*, 22(2), 193–202.
- García-Sansegundo, J., Farías, P., Gallastegui, G., Giacosa, R. E., & Heredia, N. (2009). Structure and metamorphism of the Gondwanan basement in the Bariloche region (North Patagonian Argentine Andes). *International Journal of Earth Sciences*, 98(7), 1599–1608. <https://doi.org/10.1007/s00531-008-0330-3>
- Gardés, E., Jaoul, O., Montel, J. -M., Seydoux-Guillaume, A. -M., & Wirth, R. (2006). Pb diffusion in monazite: An experimental study of Pb<sup>2+</sup>+Th<sup>4+</sup>↔2Nd<sup>3+</sup> interdiffusion. *Geochimica et Cosmochimica Acta*, 70(9), 2325–2336. <https://doi.org/10.1016/j.gca.2006.01.018>
- Gasser, D., Jęřábek, P., Faber, C., Stünitz, H., Menegon, L., Corfu, F., et al. (2015). Behaviour of geochronometers and timing of metamorphic reactions during deformation at lower crustal conditions: Phase equilibrium modelling and U-Pb dating of zircon, monazite, rutile and titanite from the Kalak Nappe Complex, northern Norway. *Journal of Metamorphic Geology*, 33(5), 513–534. <https://doi.org/10.1111/jmg.12131>
- Giacosa, R., Heredia, N., Césari, O., & Zubía, M. (2001). *Hoja 4172-IV, San Carlos de Bariloche (provincias de Río Negro y Bariloche)*. Buenos Aires: Instituto de Geología y Recursos Minerales (IGRM) – SEGEMAR.
- Giacosa, R., Márquez, M., Nillni, A., Fernández, M., Fracchia, D., Parisi, C., et al. (2004). Litología y estructura del basamento ígneo-metamórfico del borde SO del Macizo Nordpatagónico al oeste del río Chico, (Cushamen, Chubut, 42° 10' S - 70° 30' O). *Revista de la Asociación Geológica Argentina*, 59(4), 569–577.
- Giacosa, R., Zubía, M., Sánchez, M., & Allard, J. (2010). Meso-Cenozoic tectonics of the southern Patagonian foreland: Structural evolution and implications for Au-Ag veins in the eastern Deseado Region (Santa Cruz, Argentina). *Journal of South American Earth Sciences*, 30(3-4), 134–150. <https://doi.org/10.1016/j.jsames.2010.09.002>
- Giacosa, R. E., Afonso, J., Heredia, N. C., & Paredes, J. (2005). Tertiary tectonics of the sub-Andean region of the North Patagonian Andes, southern central Andes of Argentina (41–42°30'S). *Journal of South American Earth Sciences*, 20(3), 157–170. <https://doi.org/10.1016/j.jsames.2005.05.013>
- Giacosa, R. E., & Heredia, N. (2004). Estructura de los Andes Nordpatagónicos en los cordones Piltriquitrón y Serrucho y en el valle de El Bolsón (41° 30'–42° 00'S), Río Negro. *Revista de la Asociación Geológica Argentina*, 59(1), 91–102.
- Gianni, G. M., Dávila, F. M., Echaurren, A., Fennell, L., Tobal, J., Navarrete, C., et al. (2018). A geodynamic model linking Cretaceous orogeny, arc migration, foreland dynamic subsidence and marine ingression in southern South America. *Earth-Science Reviews*, 185, 437–462. <https://doi.org/10.1016/j.earscirev.2018.06.016>
- Goncalves, P., Oliot, E., Marquer, D., & Connolly, J. A. D. (2012). Role of chemical processes on shear zone formation: an example from the Grimsel metagranodiorite (Aar massif, Central Alps). *Journal of Metamorphic Geology*, 30(7), 703–722. <https://doi.org/10.1111/j.1525-1314.2012.00991.x>
- González Bonorino, F. (1973). *Geología entre San Carlos de Bariloche y Llao Llao*. San Carlos de Bariloche: Fundación Bariloche.
- González Díaz, E. F. (1982). Chronological zonation of granitic plutonism in the Northern Patagonian Andes of Argentina: The migration of intrusive cycles. *Earth-Science Reviews*, 18(3-4), 365–393. [https://doi.org/10.1016/0012-8252\(82\)90045-9](https://doi.org/10.1016/0012-8252(82)90045-9)
- González, P. D., Sato, A. M., Naipauer, M., Varela, R., Basei, M., Sato, K., et al. (2018). Patagonia-Antarctica Early Paleozoic conjugate margins: Cambrian synsedimentary silicic magmatism, U-Pb dating of K-bentonites, and related volcanogenic rocks. *Gondwana Research*, 63, 186–225.
- González, P. D., Tortello, F., & Damborenea, S. (2011). Early Cambrian Archaeocyathan limestone blocks in low-grade metaconglomerate from El Jagüelito Formation (Sierra Grande, Río Negro, Argentina). *Geologica Acta*, 9(2), 159–163.
- González, P. D., Tortello, M., Damborenea, S., Naipauer, M., Sato, A. M., & Varela, R. (2012). Archaeocyaths from South America: Review and new record. *Geological Journal*, 48, 114–125.

- Goscombe, B. D., & Gray, D. R. (2009). Metamorphic response in orogens of different obliquity, scale and geometry. *Gondwana Research*, 15(2), 151–167. <https://doi.org/10.1016/j.gr.2008.07.005>
- Greco, R. (1975). *Hoja 40a, Monte Tronador, provincia de Río Negro*. Buenos Aires: Servicio Geológico Nacional.
- Gregori, D. A., Kostadinoff, J., Strazzere, L., & Raniolo, A. (2008). Tectonic significance and consequences of the Gondwanide orogeny in northern Patagonia, Argentina. *Gondwana Research*, 14(3), 429–450. <https://doi.org/10.1016/j.gr.2008.04.005>
- Gregori, D. A., Saini-Eidukat, B., Benedini, L., Strazzere, L., Barros, M., & Kostadinoff, J. (2016). The Gondwana orogeny in northern north Patagonian massif: Evidences from the Caita C6 granite, La Seña and Pangaré mylonites, Argentina. *Geoscience Frontiers*, 7(4), 621–638. <https://doi.org/10.1016/j.gsf.2015.06.002>
- Harlov, D. E., Wirth, R., & Hetherington, C. J. (2011). Fluid-mediated partial alteration of monazite: The role of coupled dissolution-precipitation during apparent solid state element mass transfer. *Contributions to Mineralogy and Petrology*, 162(2), 329–348. <https://doi.org/10.1007/s00410-010-0599-7>
- Heredia, N., García-Sanseguendo, J., Gallastegui, G., Farias, P., Giacosa, R., Hongn, F., et al. (2018). The Pre-Andean phases of construction of the Southern Andes basement in Neoproterozoic-Paleozoic times. In A. Folguera, E. C. Reyes, N. Heredia, A. Encinas, S. Iannelli, V. Oliveros, F. Dávila, G. Collo, L. Giambiagi, A. Maksymowicz, P. I. Llanos, M. Turienzo, M. Naipauer, D. M. Orts, V. Litvak, O. Alvarez, & C. Arriagada (Eds.), *The Evolution of the Chilean-Argentinean Andes*, (pp. 133–153). Cham: Springer International Publishing AG.
- Heredia, N., García-Sanseguendo, J., Gallastegui, G., Farias, P., Giacosa, R. E., Giambiagi, L. B., et al. (2017). Review of the geodynamic evolution of the SW margin of Gondwana preserved in the Central Andes of Argentina and Chile (28°–38°S latitude). *Journal of South American Earth Sciences*, 87, 87–94. <https://doi.org/10.1016/j.jsames.2017.11.019>
- Hervé, F., Calderon, M., Fanning, C. M., Pankhurst, R. J., Fuentes, F., Rapela, C. W., et al. (2016). Devonian magmatism in the accretionary complex of southern Chile. *Journal of the Geological Society*, 173(4), 587–602. <https://doi.org/10.1144/jgs2015-163>
- Hervé, F., Calderón, M., Fanning, C. M., Pankhurst, R. J., & Godoy, E. (2013). Provenance variations in the Late Paleozoic accretionary complex of central Chile as indicated by detrital zircons. *Gondwana Research*, 23(3), 1122–1135. <https://doi.org/10.1016/j.gr.2012.06.016>
- Hervé, F., Calderon, M., Fanning, C. M., Pankhurst, R. J., Rapela, C. W., & Quezada, P. (2018). The country rocks of Devonian magmatism in the north Patagonian massif and Chaitenia. *Andean Geology*, 45(3), 301–317. <https://doi.org/10.5027/andgeoV45n3-3117>
- Hervé, F., Haller, M. J., Duhart, P., & Fanning, C. M. (2005). SHRIMP U-Pb ages of detrital zircons from Cushamen and Esquel formations, North Patagonian Massif, Argentina: Geological implications. Paper presented at the XVI Congreso Geológico Argentino, La Plata, Argentina.
- Hobbs, B. E., Ord, A., & Regenauer-Lieb, K. (2011). The thermodynamics of deformed metamorphic rocks: A review. *Journal of Structural Geology*, 33(5), 758–818. <https://doi.org/10.1016/j.jsg.2011.01.013>
- Holdaway, M. J. (2000). Application of new experimental and garnet Margules data to the garnet-biotite geothermometer. *American Mineralogist*, 85(7-8), 881–892. <https://doi.org/10.2138/am-2000-0701>
- Horton, B. K. (2018). Sedimentary record of Andean mountain building. *Earth-Science Reviews*, 178, 279–309. <https://doi.org/10.1016/j.earscirev.2017.11.025>
- Iannelli, S. B., Litvak, V. D., Fernández Paz, L., Folguera, A., Ramos, M. E., & Ramos, V. A. (2017). Evolution of Eocene to Oligocene arc-related volcanism in the North Patagonian Andes (39–41°S), prior to the break-up of the Farallon plate. *Tectonophysics*, 696–697, 70–87. <https://doi.org/10.1016/j.tecto.2016.12.024>
- Janots, E., Brunet, F., Goffé, B., Poinssot, C., Burchard, M., & Cemic, L. (2007). Thermochemistry of monazite-(La) and dissakisite-(La): Implications for monazite and allanite stability in metapelites. *Contributions to Mineralogy and Petrology*, 154(1), 1–14. <https://doi.org/10.1007/s00410-006-0176-2>
- Japas, M. S., Sruoga, P., Kleiman, L. E., Gayone, M. R., Maloberti, A., & Comito, O. (2013). Cinemática de la extensión jurásica vinculada a la provincia silícea Chon Aike, Santa Cruz, Argentina. *Revista de la Asociación Geológica Argentina*, 70(1), 16–30.
- Japas, M. S., Vizán, H., Prezzi, C., Geune, S. E., Franzese, J., Renda, E., & Oriolo, S. (2017). Pangea, autosubducción y cuencas extensionales mesozoicas del margen sudoeste de Gondwana. Paper presented at the XX Congreso Geológico Argentino, San Miguel de Tucumán, Argentina.
- Johnson, S. E. (1999). Porphyroblast microstructures: A review of current and future trends. *American Mineralogist*, 84(11-12), 1711–1726. <https://doi.org/10.2138/am-1999-11-1202>
- Jones, R. R., Holdsworth, R. E., Clegg, P., Tavarnelli, E., & McCaffrey, K. J. W. (2004). Inclined transpression. *Journal of Structural Geology*, 26(8), 1531–1548. <https://doi.org/10.1016/j.jsg.2004.01.004>
- Just, J., Schulz, B., de Wall, H., Jourdan, F., & Pandit, M. K. (2010). Monazite CHIME/EPMA dating of Erinpura granitoid deformation: Implications for Neoproterozoic tectono-thermal evolution of NW India. *Gondwana Research*, 19(2), 402–412. <https://doi.org/10.1016/j.gr.2010.08.002>
- Kato, T. T., Sharp, W., & Godoy, E. (2008). Inception of a Devonian subduction zone along the southwestern Gondwana margin: <sup>40</sup>Ar/<sup>39</sup>Ar dating of eclogite-amphibolite assemblage in blueschist boulders from the coastal range of Chile (41°S). *Canadian Journal of Earth Sciences*, 45(3), 337–351. <https://doi.org/10.1139/E08-006>
- Keidel, H. (1938). Über die “Gondwaniden” Argentinien. *Geologische Rundschau*, 30(1), 148–240.
- Kelsey, D. E., Clark, C., & Hand, M. (2008). Thermobarometric modelling of zircon and monazite growth in melt-bearing systems: Examples using model metapelitic and metapsammitic granulites. *Journal of Metamorphic Geology*, 26(2), 199–212. <https://doi.org/10.1111/j.1525-1314.2007.00757.x>
- López de Luchi, M. G., & Cerredo, M. E. (2008). Geochemistry of the Mamil Choique granitoids at Río Chico, Río Negro, Argentina: Late Paleozoic crustal melting in the north Patagonian massif. *Journal of South American Earth Sciences*, 25(4), 526–546. <https://doi.org/10.1016/j.jsames.2007.05.004>
- Lucassen, F., Trumbull, R., Franz, G., Creixell, C., Vázquez, P., Romer, R. L., & Figueroa, O. (2004). Distinguishing crustal recycling and juvenile additions at active continental margins: the Paleozoic to recent compositional evolution of the Chilean Pacific margin (36–41 S). *Journal of South American Earth Sciences*, 17(2), 103–119.
- Ludwig, K. R. (2001). *User manual for Isoplot/Ex (rev. 2.49): A geochronological toolkit for Microsoft Excel*. Berkeley: Berkeley Geochronology Center Special Publication.
- Marcos, P., Gregori, D. A., Benedini, L., Barros, M., Strazzere, L., & Pavón Pivetta, C. (2018). Pennsylvanian glacial marine sedimentation in the Cushamen Formation, western north Patagonian massif. *Geoscience Frontiers*, 9(2), 485–504. <https://doi.org/10.1016/j.gsf.2017.05.005>
- Marsh, J. H., Johnson, S. E., Yates, M. G., & West, D. P. Jr. (2009). Coupling of deformation and reactions during mid-crustal shear zone development: An in situ frictional-viscous transition. *Journal of Metamorphic Geology*, 27(8), 531–553. <https://doi.org/10.1111/j.1525-1314.2009.00841.x>

- Martin, M. W., Kato, T. T., Rodríguez, C., Godoy, E., Duhart, P., McDonough, M., & Campos, A. (1999). Evolution of the late Paleozoic accretionary complex and overlying forearc-magmatic arc, south central Chile (38°–41°S): Constraints for the tectonic setting along the southwestern margin of Gondwana. *Tectonics*, *18*(4), 582–605. <https://doi.org/10.1029/1999TC900021>
- Martínez Dopico, C. I., Tohver, E., López de Luchi, M. G., Wemmer, K., Rapalini, A. E., & Cawood, P. A. (2017). Jurassic cooling ages in Paleozoic to early Mesozoic granitoids of northeastern Patagonia: <sup>40</sup>Ar/<sup>39</sup>Ar, <sup>40</sup>K-<sup>40</sup>Ar mica and U-Pb zircon evidence. *International Journal of Earth Sciences*, *106*(7), 2343–2357. <https://doi.org/10.1007/s00531-016-1430-0>
- Martínez, J. C., Dristas, J. A., & Massonne, H. -J. (2012). Palaeozoic accretion of the microcontinent Chilenia, North Patagonian Andes: high-pressure metamorphism and subsequent thermal relaxation. *International Geology Review*, *54*(4), 472–490. <https://doi.org/10.1080/00206814.2011.569411>
- Montel, J. M., Foret, S., Veschambre, M., Nicollet, C., & Provost, A. (1996). Electron microprobe dating of monazite. *Chemical Geology*, *131*(1-4), 37–53. [https://doi.org/10.1016/0009-2541\(96\)00024-1](https://doi.org/10.1016/0009-2541(96)00024-1)
- Mulch, A., & Cosca, M. A. (2004). Recrystallization or cooling ages: In situ UV-laser <sup>40</sup>Ar/<sup>39</sup>Ar geochronology of muscovite in mylonitic rocks. *Journal of the Geological Society*, *161*(4), 573–582. <https://doi.org/10.1144/0016-764903-110>
- Müller, R. D., Seton, M., Zahirovic, S., Williams, S. E., Matthews, K. J., Wright, N. M., et al. (2016). Ocean basin evolution and global-scale plate reorganization events since Pangea breakup. *Annual Review of Earth and Planetary Sciences*, *44*(1), 107–138. <https://doi.org/10.1146/annurev-earth-060115-012211>
- Naipauer, M., García Morabito, E., Marques, J. C., Tunik, M., Rojas Vera, E. A., Vujovich, G. I., et al. (2012). Intraplate Late Jurassic deformation and exhumation in western central Argentina: Constraints from surface data and U-Pb detrital zircon ages. *Tectonophysics*, *524*–*525*, 59–75. <https://doi.org/10.1016/j.tecto.2011.12.017>
- Navarrete, C., Gianni, G., Echaurren, A., Lince Klínger, F., & Folguera, A. (2016). Episodic Jurassic to Lower Cretaceous intraplate compression in Central Patagonia during Gondwana breakup. *Journal of Geodynamics*, *102*, 185–201. <https://doi.org/10.1016/j.jog.2016.10.001>
- Navarrete, C. R., Gianni, G., Echaurren, A., & Folguera, A. (2018). Lower Jurassic to Early Paleogene intraplate contraction in Central Patagonia. In A. Folguera, E. C. Reyes, N. Heredia, A. Encinas, S. Iannelli, V. Oliveros, F. Dávila, G. Collo, L. Giambiagi, A. Maksymowicz, P. I. Llanos, M. Turienzo, M. Naipauer, D. M. Orts, V. Litvak, O. Alvarez, & C. Arriagada (Eds.), *The Evolution of the Chilean-Argentinean Andes*, (pp. 245–271). Cham: Springer International Publishing AG.
- Oriolo, S., Oyhançabal, P., Wemmer, K., Basei, M. A. S., Benowitz, J., Pfänder, J., et al. (2016). Timing of deformation in the Sarandí del Yí Shear Zone, Uruguay: Implications for the amalgamation of western Gondwana during the Neoproterozoic Brasiliano-Pan-African orogeny. *Tectonics*, *35*, 754–771. <https://doi.org/10.1002/2015TC004052>
- Oriolo, S., Wemmer, K., Oyhançabal, P., Fossen, H., Schulz, B., & Siegesmund, S. (2018). Geochronology of shear zones—A review. *Earth-Science Reviews*, *185*, 665–683. <https://doi.org/10.1016/j.earscirev.2018.07.007>
- Orts, D. L., Folguera, A., Encinas, A., Ramos, M., Tobal, J., & Ramos, V. A. (2012). Tectonic development of the North Patagonian Andes and their related Miocene foreland basin (41°30'–43°S). *Tectonics*, *31*, TC3012. <https://doi.org/10.1029/2011TC003084>
- Oyhançabal, P., Wegner-Eimer, M., Wemmer, K., Schulz, B., Frei, R., & Siegesmund, S. (2012). Paleo- and Neoproterozoic magmatic and tectonometamorphic evolution of the Isla Cristalina de Rivera (Nico Pérez Terrane, Uruguay). *International Journal of Earth Sciences*, *101*(7), 1745–1762. <https://doi.org/10.1007/s00531-012-0757-4>
- Páez, G. N., Ruiz, R., Guido, D. M., Jovic, S. M., & Schalamuk, I. B. (2011). Structurally controlled fluid flow: High-grade silver ore-shoots at Martha epithermal mine, Deseado massif, Argentina. *Journal of Structural Geology*, *33*(5), 985–999. <https://doi.org/10.1016/j.jsg.2011.02.007>
- Pankhurst, R. J., Rapela, C., López de Luchi, M. G., Rapalini, A. E., Fanning, C. M., & Galindo, C. (2014). The Gondwana connections of northern Patagonia. *Journal of the Geological Society*, *171*(3), 313–328. <https://doi.org/10.1144/jgs2013-081>
- Pankhurst, R. J., Rapela, C. W., Fanning, C. M., & Márquez, M. (2006). Gondwanide continental collision and the origin of the Patagonia. *Earth-Science Reviews*, *76*(3-4), 235–257. <https://doi.org/10.1016/j.earscirev.2006.02.001>
- Pankhurst, R. J., Riley, T. R., Fanning, C. M., & Kelley, S. P. (2000). Episodic silicic volcanism in Patagonia and the Antarctic Peninsula: Chronology of magmatism associated with the break-up of Gondwana. *Journal of Petrology*, *41*(5), 605–625. <https://doi.org/10.1093/ptrology/41.5.605>
- Poitrasson, F., Chenery, S., & Bland, D. J. (1996). Contrasted monazite hydrothermal alteration mechanisms and their geochemical implications. *Earth and Planetary Science Letters*, *145*(1-4), 79–96. [https://doi.org/10.1016/S0012-821X\(96\)00193-8](https://doi.org/10.1016/S0012-821X(96)00193-8)
- Ponce, C., Druguet, E., & Carreras, J. (2013). Development of shear zone-related lozenges in foliated rocks. *Journal of Structural Geology*, *50*, 176–186. <https://doi.org/10.1016/j.jsg.2012.04.001>
- Powell, R., & Holland, T. J. B. (1994). Optimal geothermometry and geobarometry. *American Mineralogist*, *79*(1-2), 120–133.
- Powell, R., & Holland, T. J. B. (2008). On thermobarometry. *Journal of Metamorphic Geology*, *26*(2), 155–179. <https://doi.org/10.1111/j.1525-1314.2007.00756.x>
- Prezzi, C., Vizán, H., Renda, E., Vázquez, S., Oriolo, S., & Japas, M. S. (2018). Evolution of the Paleozoic Claromecó Basin (Argentina) and geodynamic implications for the southwestern margin of Gondwana: Insights from isostatic, gravimetric and magnetometric models. *Tectonophysics*, *742*–*743*, 120–136. <https://doi.org/10.1016/j.tecto.2018.05.025>
- Profeta, L., Ducea, M. N., Chapman, J. B., Paterson, S. R., Henriquez Gonzales, S. M., Kirsch, M., et al. (2015). Quantifying crustal thickness over time in magmatic arcs. *Scientific Reports*, *5*, 17786. <https://doi.org/10.1038/srep17786>
- Pyle, J. M., Spear, F. S., Rudnick, R. L., & McDonough, W. F. (2001). Monazite-xenotime-garnet equilibrium in metapelites and a new monazite-garnet thermometer. *Journal of Petrology*, *42*(11), 2083–2107. <https://doi.org/10.1093/ptrology/42.11.2083>
- Quezada, P. A. (2015). Geología del basamento de la Región de los Lagos, Chile; evidencias de magmatismo calco-alcalino y aportes sedimentarios devónicos (master's thesis). Repositorio de la Universidad de Chile. Santiago de Chile, Universidad de Chile. Retrieved from (<http://repositorio.uchile.cl/handle/2250/133541>)
- Raimondo, T., Collins, A. S., Hand, M., Walker-Hallam, A., Hugh Smithies, R., Evins, P. M., & Howard, H. M. (2010). The anatomy of a deep intracontinental orogen. *Tectonics*, *29*, TC4024. <https://doi.org/10.1029/2009TC002504>
- Ramos, V. A. (1984). Patagonia: ¿Un continente paleozoico a la deriva? Paper presented at IX Congreso Geológico Argentino, San Carlos de Bariloche, Argentina.
- Ramos, V. A. (2008). Patagonia: A paleozoic continent adrift? *Journal of South American Earth Sciences*, *26*(3), 235–251. <https://doi.org/10.1016/j.jsames.2008.06.002>
- Ramos, V. A., Folguera, A., & García Morabito, E. (2011). Las provincias geológicas del Neuquén. In H. A. Lesanza, C. Arregui, O. Carbone, J. C. Danielli, & J. M. Vallés (Eds.), *Relatorio del XVIII Congreso Geológico Argentino*, (pp. 317–326). Neuquén: Asociación Geológica Argentina.

- Ramos, V. A., & Naipauer, M. (2014). Patagonia: Where does it come from? *Journal of Iberian Geology*, *40*, 367–379.
- Rapalini, A. E., López de Luchi, M., Martínez Dopico, C., Lince Klinger, F., Giménez, M., & Martínez, P. (2010). Did Patagonia collide with Gondwana in the Late Paleozoic? Some insights from a multidisciplinary study of magmatic units of the north Patagonian massif. *Geologica Acta*, *8*(4), 349–371. <https://doi.org/10.1344/105.000001577>
- Rapalini, A. E., López de Luchi, M., Tohver, E., & Cawood, P. A. (2013). The South American ancestry of the North Patagonian Massif: Geochronological evidence for an autochthonous origin? *Terra Nova*, *25*(4), 337–342. <https://doi.org/10.1111/ter.12043>
- Rapela, C. W., Pankhurst, R. J., Fanning, C. M., & Hervé, F. (2005). Pacific subduction coeval with the Karoo mantle plume: The Early Jurassic Subcordilleran belt of northwestern Patagonia. In A. R. M. Vaughan, P. Y. Leat, & R. J. Pankhurst (Eds.), *Terrane processes at the margins of Gondwana*, (Vol. 246, pp. 217–239). London: Geological Society of London.
- Rapela, C. W., Spalletti, L. A., Merodio, J. C., & Aragón, E. (1988). Temporal evolution and spatial variation of early Tertiary volcanism in the Patagonian Andes (40°S–42°30'S). *Journal of South American Earth Sciences*, *1*(1), 75–88. [https://doi.org/10.1016/0895-9811\(88\)90017-X](https://doi.org/10.1016/0895-9811(88)90017-X)
- Reimer, W., Miller, H., & Mehl, H. (1996). Mesozoic and Cenozoic palaeo-stress fields of the south Patagonian massif deduced from structural and remote sensing data. In B. C. Storey, E. C. King, & R. A. Livermore (Eds.), *Weddell Sea tectonics and Gondwana break-up*, (Vol. 108, pp. 73–85). London: Geological Society of London.
- Renda, E., Oriolo, S., & Vizán, H. (2017). Comparación estructural entre dos unidades de la Formación Mamil Choique: granitoide de Sierra del Medio (~253 Ma) y granodiorita Paso del Sapo (~314 Ma). Paper presented at the XX Congreso Geológico Argentina, San Miguel de Tucumán, Argentina.
- Schulz, B. (2017). Polymetamorphism in garnet micaschists of the Saualpe Eclogite Unit (Eastern Alps, Austria), resolved by automated SEM methods and EMP-Th-U-Pb monazite dating. *Journal of Metamorphic Geology*, *35*(2), 141–163. <https://doi.org/10.1111/jmg.12224>
- Serra-Varela, S., González, P. D., Giacosa, R. E., Heredia, N., Pedreira, D., Martín-González, F., & Sato, A. M. (2018). The poly-orogenic Palaeozoic basement of the Northpatagonian Andes in the San Martín de los Andes area (Neuquén, Argentina): Characteristics, age and correlations. *Andean Geology*, *46*(1), 102. <https://doi.org/10.5027/andgeoV46n1-3124>
- Serra-Varela, S., González, P. D., Giacosa, R. E., Heredia, N., & Sato, A. M. (2017). Condiciones físicas del metamorfismo de alta temperatura y baja presión del basamento paleozoico inferior en el área de San Martín de los Andes, Neuquén. Paper presented at XX Congreso Geológico Argentino, Córdoba, Argentina.
- Silvestro, J., & Zubiri, M. (2008). Convergencia oblicua: modelo estructural alternativo para la Dorsal Neuquina (39°S)-Neuquén. *Revista de la Asociación Geológica Argentina*, *63*(1), 49–64.
- Skrzypek, E., Schulmann, K., Štípská, P., Chopin, F., Lehmann, J., Lexa, O., & Haloda, J. (2011). Tectono-metamorphic history recorded in garnet porphyroblasts: Insights from thermodynamic modelling and electron backscatter diffraction analysis of inclusion trails. *Journal of Metamorphic Geology*, *29*(4), 473–496. <https://doi.org/10.1111/j.1525-1314.2010.00925.x>
- Somoza, R., & Zafaranna, C. B. (2008). Mid-Cretaceous polar standstill of South America, motion of the Atlantic hotspots and the birth of the Andean cordillera. *Earth and Planetary Science Letters*, *271*(1–4), 267–277. <https://doi.org/10.1016/j.epsl.2008.04.004>
- Spear, F. S. (1993). *Metamorphic phase equilibria and pressure-temperature-time paths*. Washington: Mineralogical Society of America Monograph Series, Washington.
- Spear, F. S. (2010). Monazite-allanite phase relations in metapelites. *Chemical Geology*, *279*(1–2), 55–62. <https://doi.org/10.1016/j.chemgeo.2010.10.004>
- Suárez, R. J., & González, P. D. (2018). Caracterización geológica del metamorfismo diastaternal mesozoico en la Cuenca Neuquina y su relación con la anomalía térmica en el sinrift. *Revista de la Asociación Geológica Argentina*, *75*(3), 457–472.
- Suzuki, K., Adachi, M., & Kajizuka, I. (1994). Electron microprobe observations of Pb diffusion in metamorphosed detrital monazites. *Earth and Planetary Science Letters*, *128*(3–4), 391–405. [https://doi.org/10.1016/0012-821X\(94\)90158-9](https://doi.org/10.1016/0012-821X(94)90158-9)
- Tchat, D. T., Schulz, B., & Nzenti, J. -P. (2009). Electron microprobe dating and thermobarometry of Neoproterozoic metamorphic events in the Kekem area, Central African Fold Belt of Cameroon. *Neues Jahrbuch für Mineralogie – Abhandlungen*, *186*(1), 95–109. <https://doi.org/10.1127/0077-7757/2009/0140>
- Teufel, S., & Heinrich, W. (1997). Partial resetting of the U-Pb isotope system in monazite through hydrothermal experiments: An SEM and U-Pb isotope study. *Chemical Geology*, *137*(3–4), 273–281. [https://doi.org/10.1016/S0009-2541\(96\)00161-1](https://doi.org/10.1016/S0009-2541(96)00161-1)
- Turner, J. C. M. (1965). Estratigrafía de Aluminé y adyacencias (provincia del Neuquén). *Revista de la Asociación Geológica Argentina*, *20*(2), 153–181.
- Urraza, I., Delpino, S., & Grecco, L. (2015). Counterclockwise post-emplacment evolution of metatrololites from Aluminé igneous-metamorphic Complex, Neuquén, Argentina. *Andean Geology*, *42*(1), 36–55.
- Urraza, I. A., Grecco, L. E., Delpino, S. H., & Arrese, M. L. (2008). Determination of rock ages by chemical analysis of Th, U, Pb in the mineral monazite (Ce, La, Th, REE, U)PO<sub>4</sub> using EPMA. Paper presented at Annual General Meeting and Research Day, Halifax, Canada.
- Urraza, I. A., Grecco, L. E., Delpino, S. H., Arrese, M. L., & Rapela, C. W. (2011). Petrología y estructura del C complejo igneo-metamórfico Aluminé, provincia de Neuquén, Argentina. *Andean Geology*, *38*(1), 98–118.
- Varela, R., Basei, M. A. S., Cingolani, C. A., Siga, O. Jr., & Passarelli, C. R. (2005). El basamento cristalino de los Andes norpatagónicos en Argentina: Geocronología e interpretación tectónica. *Revista Geológica de Chile*, *32*(2), 167–187. <https://doi.org/10.4067/S0716-02082005000200001>
- Varela, R., Gregori, D. A., González, P. D., & Basei, M. A. S. (2015). Caracterización geoquímica del magmatismo de arco devónico y carbonífero-pérmico en el noroeste de Patagonia, Argentina. *Revista de la Asociación Geológica Argentina*, *72*(3), 419–432.
- Villa, I. M., Bucher, S., Bousquet, R., Kleinhanns, I. C., & Schmid, S. M. (2014). Dating polygenetic metamorphic assemblages along a transect across the Western Alps. *Journal of Petrology*, *55*(4), 803–830. <https://doi.org/10.1093/ptrology/egu007>
- Vizán, H., Prezzi, C., Japas, M. S., Van Zele, M. A., Geuna, S. E., & Renda, E. M. (2015). Tracción de losa en el margen boreal del Océano Paleotetis y deformación en el interior de Gondwana (incluyendo el cordón plegado de Ventana). *Revista de la Asociación Geológica Argentina*, *72*(9), 355–377.
- Vizán, H., Prezzi, C. B., Geuna, S. E., Japas, M. S., Renda, E. M., Franzese, J., & van Zele, M. A. (2017). Paleotethys slab pull, self-lubricated weak lithospheric zones, poloidal and toroidal plate motions, and Gondwana tectonics. *Geosphere*, *13*(5), 1541–1554. <https://doi.org/10.1130/GES01444.1>
- von Gosen, W. (2003). Thrust tectonics in the north Patagonian massif (Argentina): Implications for a Patagonia plate. *Tectonics*, *22*(1), 1005. <https://doi.org/10.1029/2001TC901039>
- von Gosen, W. (2009). Stages of Late Palaeozoic deformation and intrusive activity in the western part of the north Patagonian massif (southern Argentina) and their geotectonic implications. *Geological Magazine*, *146*(1), 48–71. <https://doi.org/10.1017/S0016756808005311>

- von Gosen, W., & Loske, W. (2004). Tectonic history of the Calcatapul Formation, Chubut province, Argentina, and the "Gastre fault system". *Journal of South American Earth Sciences*, *18*(1), 73–88. <https://doi.org/10.1016/j.jsames.2004.08.007>
- Wallis, D., Lloyd, G. E., Phillips, R. J., Parsons, A. J., & Walshaw, R. D. (2015). Low effective fault strength due to frictional-viscous flow in phyllonites, Karakoram Fault Zone, NW India. *Journal of Structural Geology*, *77*, 45–61. <https://doi.org/10.1016/j.jsg.2015.05.010>
- Wehrens, P., Berger, A., Peters, M., Spillmann, T., & Herwegh, M. (2016). Deformation at the frictional-viscous transition: Evidence for cycles of fluid-assisted embrittlement and ductile deformation in the granitoid crust. *Tectonophysics*, *693*, 66–84. <https://doi.org/10.1016/j.tecto.2016.10.022>
- Williams, M. L., & Jercinovic, M. J. (2012). Tectonic interpretation of metamorphic tectonites: Integrating compositional mapping, microstructural analysis and *in situ* monazite dating. *Journal of Metamorphic Geology*, *30*(7), 739–752. <https://doi.org/10.1111/j.1525-1314.2012.00995.x>
- Willner, A. P., Gerdes, A., Massonne, H. -J., Schmidt, A., Sudo, M., Thomson, S. N., & Vujovich, G. (2011). The geodynamics of collision of a microplate (Chilenia) in Devonian times deduced by the pressure-temperature-time evolution within part of a collisional belt (Guarguaraz Complex, W-Argentina). *Contributions to Mineralogy and Petrology*, *162*(2), 303–327. <https://doi.org/10.1007/s00410-010-0598-8>
- Willner, A. P., Glodny, J., Gerya, T. V., Godoy, E., & Massonne, H. -J. (2004). A counterclockwise *PTt* path of high-pressure/low-temperature rocks from the Coastal Cordillera accretionary complex of south-central Chile: Constraints for the earliest stage of subduction mass flow. *Lithos*, *75*(3-4), 283–310. <https://doi.org/10.1016/j.lithos.2004.03.002>
- Wu, C. M. (2015). Revised empirical garnet-biotite-muscovite-plagioclase geobarometer in metapelites. *Journal of Metamorphic Geology*, *33*(2), 167–176. <https://doi.org/10.1111/jmg.12115>
- Yakymchuk, C., & Godin, L. (2012). Coupled role of deformation and metamorphism in the construction of inverted metamorphic sequences: An example from far-northwest Nepal. *Journal of Metamorphic Geology*, *30*(5), 513–535. <https://doi.org/10.1111/j.1525-1314.2012.00979.x>
- Zappettini, E. O., Chernicoff, C. J., Santos, J. O. S., Dalponte, M., Belousova, E., & McNaughton, N. (2012). Retrowedge-related Carboniferous units and coeval magmatism in the northwestern Neuquén province, Argentina. *International Journal of Earth Sciences*, *101*(8), 2083–2104. <https://doi.org/10.1007/s00531-012-0774-3>